Fracture Stratigraphy of Mesozoic platform carbonates, Agri Valley, southern Italy

Journal:	*Geological Magazine*
Manuscript ID	Draft
Manuscript Type:	Original Article
Date Submitted by the Author:	n/a
Complete List of Authors:	Manniello, Canio; Università degli Studi della Basilicata, Department of Sciences Agosta, Fabrizio; Università degli Studi della Basilicata, Department of Sciences Todaro, Simona; Università degli Studi di Palermo, Department of Earth and Marine Sciences Cavalcante, Francesco; Consiglio Nazionale delle Ricerche, Institute of Methodologies for Environmental Analyses Prosser, Giacomo; Università degli Studi della Basilicata, Department of Sciences
Keywords:	Depositional setting, main failure modes, fracture density, fracture intensity, carbonate petrography, XRPD analysis, multiscale fracture distribution
Abstract:	The outcropping platform carbonates form a layered succession crosscut by a dense array of bed-parallel pressure solution seams and veins, oblique-to-bedding pressure solution seams, and high-angle joints, veins, and pressure solution seams. Altogether, these structural elements form sub-seismic heterogeneities that formed during the poly-phase tectonic evolution of the southern Apennines fold and-thrust belt, Italy. Aiming at assessing the role exerted by the primary carbonate architecture on failure modes and fracture geometry and distribution, we conduct a multi-disciplinary study by performing stratigraphic, petrographic, mineralogical, and mesoscale structural analyses. Based on carbonate rocks textures and fossil associations, three bed package associations associated to Pliensbachian-Toarcian, low-to-high energy open lagoonal, and Cenomanian, medium-to-high lagoonal-tidal depositional settings are assessed. Based upon specific failure modes, the aforementioned structural elements pertain to burial diagenesis, an early thrusting, a thrusting and a transtensional structural assemblages. Computed P20 (2D fracture density) and P21 (2D fracture intensity) values show that the primary interfaces present in the well bedded, low energy, open lagoonal carbonates compartmentalized fractures within single carbonate beds and bed packages. On the contrary, the aforementioned values show the absence of efficient mechanical interfaces in the medium-to-high energy lagoonal-tidal carbonates. This conclusion is confirmed by considering the P10 (1D fracture intensity) values computed for the most common diffuse fracture set. Moreover, the higher values are computed for the coarse grained lithologies, which is consistent with the control exerted by early chemical and physical compaction and cementation processes in the fracture stratigraphy of the study platform carbonates.

Università degli Studi della Basilicata
Dipartimento di Scienze

Canio Manniello
Dipartimento di Scienze
Università degli Studi della Basilicata
Via dell'Ateneo Lucano,10
85100, Potenza (Pz)
E-mail: c.manniello@unibas.it

Dear editor,

on behalf of my co-authors, I would like to submit the enclosed original article entitled "*Fracture Stratigraphy of Mesozoic platform carbonates, Agri Valley, southern Italy*" to the special Issue of the Geological Magazine journal entitled "*Faults and fractures in rocks: mechanics, occurrence, dating, stress history and fluid flow*". The present contribution includes original data obtained after stratigraphic, petrographic, mineralogical, and structural analysis of outcropping platform carbonates of southern Italy. The study sites expose Mesozoic rocks crosscut by numerous sets of meso-scale fractures, whose distribution throughout the layered succession is investigated with respect to both depositional setting and diagenetic evolution of the carbonates. Results show that platform carbonates originally deposited within lagoonal settings included well-developed primary anisotropies such as bed and bed package interfaces, which acted as mechanical barrier to the vertical development of the fracture array. Differently those originally deposited in the tidal-lagoonal setting included amalgamated carbonate beds, which did not affect the vertical fracture growth by linkage of pre-existing fractures. However, despite those differences, all study rocks show higher values of fracture density within the coarse-grained carbonate beds. Results are interpreted as due to physical-chemical compaction and cementation processes that took place within the carbonate prior to early Pleistocene transtensional faulting. Finally, a conceptual model of the main structural assemblages documented at the outcrops scale within the carbonates is reported.

I believe that our manuscript will be of interest for a broad scientific community, including geologists working in the academia and those dealing with hydrocarbon, water, and geothermal industries. For this reason, I thank you for the attention. and look forward to receive your comments and suggestions.

Best Regards,

Canio Manniello, Ph.D. student

Hereafter, I include the list of possible reviewers of the accompanying manuscript with their respective main topics of interest:

1. Dr. Andrea Billi, Italian Council of Research, Rome, Italy. – Tectonics, Geodynamics, Structural Geology.
   andrea.billi@cnr.it

2. Dr. Arthur Lavenu, ADNOC group, Abu Dhabi, United Arab Emirates.- Rock mechanics, carbonate rocks
   alavenu@adnoc.ae

3. Dr. Fabrizio Berra, Università degli studi di Milano, Milan, Italy – Paleontology, Stratigraphy
   fabrizio.berra@unimi.it

4. Dr. Alessandro Ellero, Italian Council of Research, Pisa, Italy – Geochemistry, Structural Geology
   alessandro.ellero@igg.cnr.it

Fracture Stratigraphy of Mesozoic platform carbonates, Agri Valley, southern Italy

Manniello C.[1]*, Agosta F.[1], Todaro S.[2], Cavalcante F.[3], Prosser G.[1]

[1]Department of Science, University of Basilicata, Italy

[2] Department of Earth and Marine Sciences, University of Palermo, Italy

[3] Institute of Methodologies for Environmental Analyses - CNR, Tito Scalo (PZ), Italy.

*Corresponding author: c.manniello@unibas.it

Keywords

Depositional setting; main failure modes; fracture density; fracture intensity; carbonate petrography; XRPD analysis; multiscale fracture distribution.

Highlights

- Open-to-tidal lagoonal depositional settings assessed for the study carbonates, which were then subjected to a 4-5 km tectonic load.

- Depositional and diagenetic primary architecture affected both failure modes and fracture distribution in the carbonate multilayer.

- Fracture compartmentalization within coarse grained carbonate beds due to both physical and chemical compaction and cementation processes.

- Main failure modes associated to specific structural assemblages related burial diagenesis, early thrusting, thrusting, and transtentional faulting.

Abstract

The outcropping platform carbonates form a layered succession crosscut by a dense array of bed-parallel pressure solution seams and veins, oblique-to-bedding pressure solution seams, and high-angle joints, veins, and pressure solution seams. Altogether, these structural elements form sub-seismic heterogeneities that formed during the poly-phase tectonic evolution of the southern

Apennines fold and-thrust belt, Italy. Aiming at assessing the role exerted by the primary carbonate architecture on failure modes and fracture geometry and distribution, we conduct a multi-disciplinary study by performing stratigraphic, petrographic, mineralogical, and mesoscale structural analyses. Based on carbonate rocks textures and fossil associations, three bed package associations associated to Pliensbachian-Toarcian, low-to-high energy open lagoonal, and Cenomanian, medium-to-high lagoonal-tidal depositional settings are assessed. Based upon specific failure modes, the aforementioned structural elements pertain to burial diagenesis, an early thrusting, a thrusting and a transtensional structural assemblages. Computed P20 (2D fracture density) and P21 (2D fracture intensity) values show that the primary interfaces present in the well bedded, low energy, open lagoonal carbonates compartmentalized fractures within single carbonate beds and bed packages. On the contrary, the aforementioned values show the absence of efficient mechanical interfaces in the medium-to-high energy lagoonal-tidal carbonates. This conclusion is confirmed by considering the P10 (1D fracture intensity) values computed for the most common diffuse fracture set. Moreover, the higher values are computed for the coarse grained lithologies, which is consistent with the control exerted by early chemical and physical compaction and cementation processes in the fracture stratigraphy of the study platform carbonates.

1. Introduction

It is well known that platform carbonates form either well-layered or massive successions depending upon their depositional paleo-environment (Tucker, 1985). In particular, considering lagoonal/peritidal carbonates, they often form well-layered successions (Flügel, 2004) including micrites with low values of primary porosity (Lucia, 1983; Lucia & Fogg, 1990). In these rocks, the total amount of effective porosity is often significantly enhanced by mesoscale fractures often confined within discrete rock intervals (Odling, 1999; Korneva *et al*, 2014; Panza *et al.*, 2016; 2019) forming single mechanical units (Gross, 1993; Gross *et al.*, 1995) bounded by primary interfaces such as bed, bed package, and bed package association interfaces (Moore, 2002; Giuffrida *et al*., 2019, 2020; La Bruna *et al.*, 2020). The primary mechanical interfaces, in which bed-parallel pressure solution seams often localize (Rustichelli *et al.*,2012, 2015) inhibit the vertical fracture propagation affecting their dimensional properties and spacing distributions (Nur, 1980; Gross *et al.*, 1995; Becker *et al.*1996, Gross *et al.*, 1997). Fracture stratigraphy is the discipline that subdivides layered rocks into distinct intervals according to fracture height, density (P20, P30), intensity (P10, P21, P32), and/or failure modes (Pollard & Aydin, 1988; Dershowitz & Herda, 1992; Wu & Pollard, 1995; Antonellini *et al.*, 2008; Agosta *et al.*, 2009, 2015). Since the rock mechanical properties at times of deformation might differ from those measured in the laboratory due to diagenetic evolution, fracture stratigraphy only takes the aforementioned fracture properties into account (Laubach *et al.*, 2010).

In this work, we analyze the fracture stratigraphy of Mesozoic carbonates pertaining to the Apennine Platform exposed in the axial zone of the southern Apennines fold-and-thrust belt, ftb (Patacca & Scandone, 2007; Schettino & Turco, 2011). The study carbonates of the Viggiano Mt. area were subjected to a multi-phase tectonic evolution, which caused the formation of both diffuse and localized fractures (Cello *et al.* 1998; Maschio *et al.*, 2005). Now, for the first time, we apply a variety of methods to investigate their stratigraphic, petrographic, mineralogical, and structural settings. The results of field stratigraphic logging and both petrographic and mineralogical analyses are discussed to decipher the primary architecture, paleo-depositional environments, and diagenetic evolution of the study platform carbonates. We then focus on both qualitative and quantitative fracture analyses to assess the main failure modes, and both two-dimensional fracture density (P20) and intensity (P21) values. Results of this work are discussed in order to gain insights into the control exerted by the primary, depositional/diagenetic carbonate architecture on the geometry, distribution, and main failure modes of mesoscale fractures. Applications of this knowledge span from groundwater management and preservation (Andreo *et al.*, 2008; Marìn *et al.*, 2015; Petrella *et al.*, 2015; Corniello *et al.*, 2018) to geothermal fluid circulation (Bellani *et al.* 2004; Smeraglia *et al.*, 2021) and hydrocarbon production (Mosca & Wavrek, 2002; Shiner *et al.*, 2004).

2. Geological Setting

The southern Apennines are a portion of the Apennines fold-and-thrusts belt (f.t.b)., which extends NW-SE from southern Abruzzo-alto Molise area (Ortona-Rocca Monfina tectonic lineament, Patacca *et al.* 1992) to the Calabrian-Lucanian border (San Gineto tectonic lineament, Amodio Morelli *et al.*, 1976). The southern Apennines ftb is made up of E-to-NE vergent thrust sheets crosscut by high-angle trastensional faults (Mostardini & Merlini, 1986; Hippolyte *et al.*, 1995; Patacca & Scandone, 2007; Vezzani et al, 2010). Its present day structural configuration is due to its multi-phase tectonic evolution, which determined a non-cylindrical deformation (Menardi Noguera & Rea, 2000).

The Viggiano Mt. study area lies in the axial zone of the southern Apennines, which is bounded westward by the Tyrrhenian back-arc extensional region (Malinverno & Ryan, 1986; Kastens *et al.*, 1990; Patacca *et al.*,1992 a,b), and by the Bradanic Through including the emerged, Plio-Pleistocene foredeep basin (Patacca *et al.*, 1990; Patacca & Scandone, 2007). The axial zone of the southern Apennines ftb forms a multi-duplex in which thrust-sheets were emplaced during late-oligocene – early miocene due to combined thin- and thick-skinned tectonic styles (Mostardini & Merlini, 1986; Casero *et al.*, 1988, 1991; Monaco *et al.*, 1998; Menardi Noguera & Rea, 2000; Improta *et al.*, 2000; Shiner *et al.*, 2004;). Since late Pliocene, the axial zone of the southern

Apennines ftb was subjected to extensional tectonics (Giano *et al.*, 2000; Novellino *et al.*, 2015) associated to the Tyrrhenian Basin opening, and/or to gravitational collapse of the orogen (Cello & Mazzoli, 1998; Doglioni *et al.*, 1996; Scrocca *et al.*, 2005; Vezzani *et al.*, 2010).

The Apennine carbonate Platform occurs as a regional scale thrust sheet within the Southern Apennines ftb. It formed at the eastern margin of the Jurassic Lugurian Tethys Ocean in between the Liguride-Sicilide and Lagonegro-Molise sedimentary basins (Patacca & Scandone, 2007; Schettino & Turco, 2001). Overall, this carbonate platform included three main stratigraphic units (Vezzani *et al.*, 2010):

(1) Capri-Bulgheria Unit, representing the westernmost portion of the ancient platform, it is constituted by internal transition facies, shallow water carbonates (Triassic - Jurassic), and re-sedimented carbonates interbedded with Lower Cretaceous to Miocene marls.

(2) Alburno-Cervati Unit, the ancient platform-interior portion, it is made up of open shallow platform facies (Triassic dolomites and dolomitic limestones) topped by shallow water limestones passing upwards to Miocene slope carbonates and terrigenous deposits.

(3) Maddalena Mt. Unit, the easternmost portion of the ancient platform, which includes the transitional facies deposited in between the Alburno-Cervati Unit and the eastern Lagonegro Basin.

2.a Viggiano Mt. area

The Viggiano Mt. area is located along the NE margin of the Agri Valley, which is an intra-mountain tectonic basin filled with Quaternary fluvio-lacustrine deposits (Di Niro *et al.*, 1992). The Agri Valley basin is WNW-ESE elongated, and it is bounded by high-angle transtensional faults forming the East Agri Valley (EAFS) and Monti della Maddalena (MMFS) fault systems (Cello & Mazzoli, 1998; Cello *et al.*, 2000; Cello *et al.*; 2003; Maschio *et al.*, 2005). According to Cello & Mazzoli (1998) and Cello *et al.* (2000), the EAFS is constituted by N120E high-angle left-lateral strike-slip faults, N30E right-lateral transtensional faults, N90-110E left-lateral transtensional faults, and N130-150E left-lateral transpressional faults. Differently, Maschio *et al.* (2005), documented left-lateral transtension along the WNW-ESE-trending, left-stepping master faults, which localized dilation within the releasing jogs forming NE–SW normal faults. Transtensional faulting involved slope deposits and paleo-soils 39 and 18 ka old, respectively (Giano *et al.*, 2000), and caused the historical seismicity that characterizes the whole Agri Valley area (Mallet, 1862; Cello *et al.*, 2003, Buttinelli *et al.*,2016).

The Viggiano Mt. area is bounded southward by NW-SE transtensional faults, northeastward by NE-SW transtensional faults, and by a NW-SE striking thrust fault to north (Fig. 2). The bottom portion of the Viggiano Mt. carbonates includes lower Jurassic wackestones and packstones (“Scarrone La Macchia” site, Fig. 2b) with thick-shelled bivalve (*Lithiotis)*, green algae (*Palaeodasycladus mediterraneus),* foraminifera (*Siphoalvulina sp, Pseudocyclammina liassica,* marking the Pleinsbachian age), as documented by Lechler (2012.). These carbonates formed in a subtropical, inner platform depositional environment, and are topped by thick, massive oolites postdating the Early Toarcian Anoxic event (Caruthers *et al.*, 2013; Trecalli *et al.*, 2012; Wignall & Bond, 2008). The Albian-Cenomanian carbonates (“Il Monte” site, Fig. 2c) include thick layers of carbonate rudstones and grainstones with gastropods, bivalves, rudits (*Radiolitidae)*, and foraminifera (Lechler *et al*., 2012). The topmost portion of the exposed carbonate succession is made up of Cenomanian carbonate mudstones-to-rudstones and boundstones (*Lithocodium*), which include geopetal structures and fossils such as the *Conicorbitolina conica*, *Salpingoporella turgida* and *Caprinidae* (Lechler *et al*., 2012).

3. Methods

The present study focuses on the two main sites of "Scarrone la Macchia" and "Il Monte", which are respectively located along the southern cliff and the topmost portion of the Viggiano Mt. massif (Fig. 2). The chosen sites of investigation are bounded by large scale, high angle transtensional faults (Fig. 1). Hereafter, the main methods employed for the research work are reported.

3.a Stratigraphic analysis and rock sampling

Detailed stratigraphic logs were performed at each study site by mean of mesoscale analysis of both bed thickness and carbonate lithofacies (Dunham, 1962). In detail, beds are bounded by laterally continuous pressure solution seams and clayish interfaces. In the field, the carbonate lithofacies were assessed by using a portable magnifying lens. Samples collected from single beds were first classified according to Dunham (1962). A total of 60 samples was collected from the "Scarrone la Macchia" site, 51 samples from the "Il Monte" site for subsequent laboratory analyses. Moreover, a total of 10 cohesive samples were collected from the clay-containing carbonate bed interfaces at the bottom of the oolithic carbonate exposed at the "Scarrone la Macchia" site.

3.b Petrographic analysis

The petrographic characterization was carried out through an optical microscope (Leitz Laborlux 12 Pol) associated to the Zen software for the acquisition of photomicrographs. The textural classifications of microfacies followed Dunham (1962) and Embry & Klovan (1971). A total of 19 thin sections from the "Scarrone la Macchia" site and 14 from the "Il Monte" site were analyzed. Biostratigraphic analysis of the Lower Jurassic carbonates from the "Scarrone La Macchia" site was based on biozonal schemes and chronostratigraphic references related to the Tethyan inner-carbonate platforms (De Castro, 1991; Boufagher-Fadel, 2008, Chiocchini *et al.*, 1994; Barattolo & Romano, 2005). Biostratigraphic analysis of the Cretaceous carbonates of the "Il Monte" site followed the distribution ranges described for the Tethyan realm in previous studies (Di Stefano & Ruberti, 2000; Chiocchini *et al.*, 1994).

3.c Mineralogical analysis

20 powders obtained from "Scarrone la Macchia" site hand samples were investigated by mean of X-ray Powder Diffraction (XRPD) analysis. Particularly, the analyzed samples include cohesive clay-containing samples gathered within carbonate bed packages interfaces and carbonate samples gathered within the interface-bounding carbonate beds. We employed the Rigaku D/Max 2200 diffractometer with Θ-Θ Bragg-Bentrano geometry, equipped with CuKα radiation, automatic sample holder spinner, secondary graphite monochromator, and scintillation detector. The following instrumental conditions were adopted: power: 40 mA x 30 kV, step scan 0.02 °2Θ, speed 3s/step, divergent slit 1°and receiver slit 0.3 mm. The random powders and oriented specimens were analyzed in the angular range of 2 - 70 °2Θ and 2 - 32 °2Θ, respectively. The analyses were performed on the bulk samples, on the terrigenous component and on the < 2 μm terrigenous fraction (Table 1).

-Please insert Table 1 here-

The hand samples were first crushed. Then, one aliquot was pulverized by friction in a concentric-disk agate mill, whereas another aliquot was treated with diluted HCl (Cuadros & Altaner, 1998) to eliminate the carbonates and collect silicate component. The silicate component was washed several times with distilled water and collected by centrifugation. 0.5 of this material was manually milled by using mortar and pestle, and then used for random specimens. 1.5 g of the material was used to separate the clay fraction (<2μm) by sedimentation in beaker, according to the Stock's law. The random specimens were prepared using side loading. The clay fraction, previously saturated with 1N $MgCl_2$ solution, was used for orientated specimens by settling suspension on a glass slide (Moores & Reynolds, 1997). The specimens were analyzed air dried, ethylene glycol solvated, and then heated at 375 °C (Moore & Reynolds, 1997). Percentage of illite and ordering (R; Reichweite) of the mixed layers illite/smectite were determined (Moore & Reynolds, 1997).

3.d Structural analysis

Field structural analyses were carried out by applying the circular scanlines method, which consists of circles drawn on the rock surface delimitating a circular window (symmetric sampling area), and linear scan lines oriented parallel to beddings. Circular scanline measurements provided the number of fracture intersections, n, and the number of fracture endpoints inside the circular window, m. In All fracture traces longer than 3 cm were considered. Both strata-bound and non-strata bound high-angle fractures were measured. Outcrops were chosen based on their accessibility, dimensions (> 10 m-long), and distance from main fault zones (Rohrbaugh *et al.*, 2002; Mauldon *et al.*, 2001).

The measured m and n parameters were then respectively employed for 2D fracture density (P20) and intensity (P21) computations, according to the approach introduced by Mauldon *et al.* (2001). Fracture density represents the number of fracture trace centers per unit area ($1/m^2$), and the estimator factor is obtained from the number of fracture endpoints (m) inside the circular window by the following equation:

$$P20=m/2\pi r$$

Where “r” is the radius of the circular scan line.

Fracture intensity represents the mean total trace length of fractures per unit area (m/m^2), and the estimator is obtained from the number of fracture intersections with the circular scan line (n) by the following equation:

$$P21=n/4\pi$$

To obtain a representative estimation of the P20 and P21 values, the circular window should be sufficiently large to contain at least 30 endpoints (Rohrbaugh *et al.*, 2002).

A linear scan line is an ideal line drawn on the rock that allows detailed measurement of fracture properties and true spacing computation for single fracture sets (Giuffrida *et al.*, 2019 and references therein). The method is based on the measure of the fracture attitude and the distance from the origin of the linear scan line. This method is employed for 1D fracture intensity, P10, and true fracture spacing (S_r), calculations. True spacing is obtained by applying a trigonometric correction to the apparent spacing (S_a) measured along the scan line. The trigonometric correction considers the α and β angles, which respectively correspond to the azimuthal angle formed by the fracture strike direction and the scan line trend, and to the zenithal angle formed by the fracture dip and the scan line plunge. The true fracture spacing is given by the following equation:

$$Sr=Sr(\sin\alpha)(\cos\beta)$$

4. Results

In this chapter, data obtained from the various analyses are reported in order to first document the stratigraphic and petrography of the carbonate succession, and then document both spatial distribution, dimensional properties, and main failure modes of the fracture networks dissecting them.

4.a Carbonate stratigraphy

4.a.1 "Scarrone la Macchia" site

The ca. 56 m thick succession includes two informal units, which respectively correspond to mud-supported and oolithic limestones. The mud-supported carbonates consist of dark limestones and marly intercalations, which dip NE and show a total thickness of about 43 m (Fig.3a). There, 12 single bed packages labelled A to N bottom up are documented (Fig. 3a), which are bounded by 5-to-15 cm-thick, clay-rich carbonate interfaces including anastomosed, bed-parallel, and bed-oblique pressure solution seams. Single bed packages show fining-upwards carbonate textures. Their thickness varies from ca. 13 m (bottom) to ca. 1m (top). Within single bed packages, thick beds of coarse-grained limestones are topped by thin beds of fine-grained limestones. Single carbonate beds are delimited by laterally continuous, mm- to cm-thick bed interfaces, which might include pressure solution seams with siliciclastic films of insoluble material. Overall, we interpret this succession as forming a bed package association, as proposed for Apulian platform carbonates exposed bot in the foreland (Spalluto, 2012; Panza *et al.*, 2016, 2019) and axial portions of the southern Apennines ftb (Giuffrida *et al.*, 2020).

The ca. 13 m-thick oolithic limestones include four main bed packages (Fig. 3a) made of 40 cm- to 5 m-thick grainstone beds showing a pronounced amalgamation, and therefore lateral variation of thickness. Bed interfaces are marked by laterally continuous clusters of well-developed pressure solution seams, which were responsible for bed amalgamation. At a close view, the single pressure solution seams do not show any presence of insoluble clayish material. The bed packages interfaces are laterally continuous and include mm-thick clay-rich carbonates crosscut by pressure solution seams. We also interpret this succession as part of a single bed package association (Spalluto, 2012) bounded at the bottom by a 10 to 15 cm thick, mixed carbonate-terrigenous interface in which tiny, mm- to cm-sized elongated clasts are embedded in a fine-grained matrix.

4.a.2 "Il Monte" site

The exposed succession consists of 67 m-thick massive carbonate mudstones and grainstones, in which bedding interfaces are not laterally continuous due to bed amalgamation (Fig. 3b). The massive carbonates include bioclastic rudstone/floatstone, grainstones, and breccias forming 11 bed packages labelled A to M bottom-up (Fig 3 b). There, single clasts are mainly made up of rudist fragments (*Radiolitidae* and *Caprinae*) up to 5 cm in size (cf. Ch. 4.b). Commonly, single bed-packages show a fining upward trend, with rudstone/floatstones as base-levels topped by thinner grainstone beds. Bed-packages interfaces are represented by laterally continuous erosive, surfaces located at the bottom of the breccia beds that are locally characterized by pressure solution. Differently, single beds interfaces are generally due to isolated pressure solution seams with quite tabular shapes. We also interpret this succession as part of a single bed package association (cf. Spalluto, 2011).

4.b Carbonate petrography

4.b.1 "Scarrone la Macchia" site

The mud supported limestones include carbonate wackestones, subordinately mudstones, and packstones/grainstones. The overall microfossil assemblages contain abundant benthic foraminifera and calcareous algae (including *Haurania sp., Siphovalvulina sp., Lituosepta sp., Palaeodasycladus mediterraneus, the microproblematica Thaumatoporella parvovesiculifera* (Figs. 4 a-e). According to the biozonal scheme proposed by Chiocchini *et al.* (1994) and Boudagher-Fadel (2008), the aforementioned fossil association is consistent with an upper Sinemurian-Pliensbachian age. The secondary porosity related to fractures is or occluded by granular cement or is still open as evidenced by blue resin (Fug. 4g).

The oolithic limestones include ooids showing obliteration of the laminae due to intense micritization (Fig. 4f). However, in some cases, is possible to individuate the original fabric consisting of concentric laminae. Ooids are 500 to 1000 μm in size. Their nuclei consist of skeletal grains, peloids and in rare cases by mineral grain. An alternation of laminae (<1cm thick) made up of micrite oncoids (> 1 mm) is documented. The ooids are cemented with blocky calcite. The lacking of suture-like contact between grains is interpreted as due to not pronounced chemical compaction of the oolites. Secondary porosity is still preserved within these rocks (Fig. 4h).

4.b.2"Il Monte" site

The poorly bedded carbonates are made up of bivalve fragments, gastropods, algae, and benthic foraminifers (orbitolinids) (Figs. 5a, b, c, e.). Single rudist fragments can be more than 5 cm in size, micritized, and in some cases affected by microboring (Fig. 5b). Only one of the study thin sections shows stromatolitic laminae associated with oncoids and ostracods. In places, single grains are affected by pervasive dissolution (Fig. 5e and 5f). Both granular and meniscus cements and isopachous crust constitute the grain-supported texture of the carbonate rudstone/grainstone (Figs. 5e and 5f). Intergranular porosity is mainly filled by carbonare cements and both barren silts and sediments rich in ostracods (Fig. 5e and 5f).

4.c Mineralogical analysis

The results of the XRPD qualitative analyses are reported in Table 2, and Figs 6 and 7. In the random powder analysis of the bulk rocks, all samples mainly include calcite. Silicate component is detectable in little amount (Fig. 6a), and it is composed by quartz, feldspars (plagioclase), goethite and clay minarals such as illite, mixed-layer illite/smectite (I/S), little amounts of chlorite and kaolinite (Fig. 6b). Mixed-layers show ordered R1, with illite percentages of 80% and R3 with 90% of illite, both in cohesive limestones and interbed layers (Fig. 7; Table 2).

- Please insert Table 2 here-

4.d Fracture Density and Intensity

At the "Scarrone la macchia" site (Fig. 8a), within the mud supported bpa the values of fracture density, P20, varies from 61 m^{-2} (1m-thick carbonate wackestone bed at ca. 35 m from the base level) to 552 m^{-2} (40 cm-thick carbonate packstone bed at ca. 14 m from the base level). We note that the P20 values commonly decrease upward within single bed packages, and that they are higher in the thicker and coarser carbonate beds. In the same rocks, the P21 value varies from 10 m^{-1} (1m thick carbonate wackestone bed at ca. 35 m from the base level) to 46.7 m^{-1} (1.6m-thick carbonate grainstone bed at ca. 7 m from the base level). We note that higher P21 values are calculated for coarser-grained, grain-supported beds located at the bottom of single bed package, and that the lower P21 values are computed for the fine-grained, mud-supported carbonate beds.

The oolithic bpa is characterized by a P20 value varying from 87.6 m^{-2} (90 cm-thick carbonate grainstone at ca. 55m from the base level) to 488 m^{-2} (50 cm-thick carbonate grainstone bed at 50 m from the base level). Differently, the P21 value spans from 1.0 m^{-1} (90 cm-thick carbonate grainstone bed at 55 m from the base level) and 47.5 m^{-1} (50 cm-thick carbonate grainstone bed at 50 m from the base level). We note that the aforementioned values of P20 and P21 are related to the same carbonate beds, and that the highest values are computed for the thinner carbonate grainstone beds.

At the "Il Monte" site (Fig. 8b), within the breccia bpa, the values of fracture density, P20, vary from 43.3 m^{-2} (20 cm mudstone bed, at ca. 14 m from the base level) to 184 m^{-2} (3 m-thick bed carbonate breccia at ca.4 m from the base level). The P21 computed values vary from 8 m^{-1} (60 cm-thick packstone, at ca. 51m from the base level) to 25 m^{-1} (2 m-thick carbonate breccia level at 14 m from the base level). The higher P20 and P21 values are computed for the thicker, coarse-grained carbonate beds, whereas the lower values for thinner, mud supported carbonate beds.

Moreover, at both "Scarrone la Macchia" site and at "il Monte" the 1D fracture intensity P10 has been calculated for the JV1 set (cf. chapter 4e. below) within significant beds and the values are reported in Table 3.

- Please insert Table 3 here-

4.e Fracture network geometry

The cumulative plots of the poles of fractures measured in the field are shown as present-day data (Fig. 9a), and after bedding restoration (Fig. 9b) in equal-area, lower-hemisphere projections (Allmendinger *et al.,* 2003). Fracture data are restored by taking the attitude of single beds into account. High angle to sub-vertical fractures are documented (Fig. 9a). The poles mainly cluster around the value of N199/06 (trend/plunge), which is related to a ca. WSW-ENE striking sub-vertical set. The restored data show a main cluster of the poles around the N195/23 value, which corresponds to a WSW-ENE striking high-angle fracture set.

In order to precisely document the fracture network geometry, the aforementioned dataset is subdivided into three different subsets corresponding to the study bed package associations, respectively (Fig. 10). Five main sets are recognized in both true data and restore data plots:

- Set A, fractures striking ca. ESE-WNW;
- Set B, fractures striking ca. NW-SE;
- Set C, fractures striking ca. N-S;
- Set D, fractures striking ca. NE-SW;
- Set E, fractures striking ca. ENE-WSW.

We note that Set A shows the greatest clustering of the poles in the mud-supported bpa, forming a 68° cut-off angle with bedding, whereas it is a secondary one in the oolithic bpa (56° cut-off angle). Set B shows low values of pole-density in all study bpa's, with cut-off angles varying from 74° (mud-supported bpa) to 55° (both oolithic and breccia bpa's). Set C is not well developed in both mud-supported and breccia bpa's, whereas it forms the main fracture set in the oolithic bpa (50° cut-off angles). Set D shows low values of pole density in all the study bpa's, forming cut-off angles varying from 86° (mud-supported bpa) to 71° (breccia bpa) and 67° (oolithic bpa). Set E is mainly present in the breccia bpa, in which it forms the main fracture sets forming a 68° cut-off angle with bedding.

4.f Main Failure Modes

Two sets of pervasive, bed-parallel pressure solution seams, PSS, are localized within bed interfaces (PSS1a) and within the single carbonate beds (PSS1b). PSS1a are laterally continuous at outcrop scales, causing bed amalgamation in the oolithic bpa, whereas PSS1b are up to 10's of cm-long (Figs 11a, 11b and 11c). Four sets of bed oblique PSS are documented in the study carbonates. The PSS2 set strikes ca. N-S and forms a 70° cut-off angle with bedding. The PSS3 set strikes NW-SE and forms a 70° cut-off angle with bedding. Both PSS4a and PSS4b sets strike ca. NE-SW. PSS4a dips ca. 70° NW, whereas PSS4b dips ca. 30° SW (Figs 11b and 11d). These structural elements abut against both PSS1a and PSS1b and are localized within the single carbonate beds. Together with the PSS1b, they form anastomosed patterns visible at outcrop scales.

Four sets of open fractures and veins are documented. The JV1 set strikes ENE-WSW to ESE-WNW, includes both strata-bound and not-strata-bound open fractures and veins (Figs 11c and 11d), and forms 75°to 85° cut-off angle with bedding. Commonly, the JV1 veins are closely spaced together forming a few cm-thick swarms within single carbonate beds. The strata bound JV1 fractures and veins abut against PSS1b (Fig 11c) and PSS1a. The JV2 set strikes circa N-S and is comprised of both not strata bound, and strata bound open fractures and veins forming 70° cut off angle with bedding. These features are mainly documented in the oolithic bpa The JV3 veins are parallel to bedding and abut against JV1 (Fig 11d). We note that these bed-parallel veins are mainly located in the carbonate beds encompassing bed package interfaces and abut against the PSS4a and PSS4b structural elements. The JV4 set strikes NW-SE, is ca. perpendicular to bedding, and mainly includes strata-bound fractures abutting against PSS1a and, subordinately, PSS1b. The JV5 set strikes NE-SW, and includes bed-perpendicular, strata-bound fractures and veins abutting against PSS1a and, subordinately, PSS1b. In map view, JV4 abut against JV5 structural elements (Fig. 11e), JV1 and JV2 show mutual crosscutting relations with JV4 and JV5 structural elements (Fig. 11e), and JV2 fractures localize at the tips of JV5 fractures.

The bed-package surfaces, are often, high-strain and very narrow volumes (not more than 15 cm of thickness). Slip surfaces have been documented along those interfaces, particularly by recognizing a top-to-NE S-C-C' tectonite fabric (Fig 11f). Within those interfaces there are elongated, sigmoidal shaped carbonate clasts. The contact surfaces between the clasts are characterized by pressure solution, and within the interfaces there are films of insoluble grayish-to-greenish siliciclastic material.

4.g Multiscale fracture spacing properties

S1, S2, and S3 linear scan lines were performed along orthogonal outcrops of the "Scarrone la macchia" site (Fig. 12) exposing the mud-supported bpa Both S1 (N230E/40°) and S3 (N100E/31°) were positioned away from mesoscale fault zones, whereas S2 (N180E/25°) crosscuts a ca. N110E striking, high angle mesoscale fault zone. The poles to fractures intersected by the S1, S2 and S3 are plotted into 3 distinct equal-area, lower-hemisphere projections (Figs 12a, 12d and 12g). Two main fracture sets striking N292E and N300E are found along S1. The bi-logarithmic fracture spacing vs. cumulative number plots show an exponential (R^2 = 0.97) best-fit function for the N292 set, and a power law (R^2 = 0.93) best fit function for the N300 set (Figs. 12b and 12c). Two main fracture sets respectively striking N252E and N284E are found along the S2. The bi-logarithmic fracture spacing vs. cumulative number plots show a power law best fit function (R^2 = 0. 96, fig. 12e) for the N252 set, and an exponential distribution (R^2 = 0.93, fig. 12f) for the N284 set. Two main fracture sets respectively striking N180E and N206E are found along the S3 dataset. The bi-logarithmic fracture spacing vs. cumulative number plots show a power law best fit function (R^2 = 0.92, fig. 12h) for the N180E set, and an exponential distribution (R^2 = 0.87, fig. 12i) for the N206E set

5. Discussion

In this chapter, we first discuss the results of stratigraphic, petrographic, and mineralogical analyses to assess the paleo depositional environments and diagenetic conditions of the carbonate sediments. Then, we consider the main failure modes in light of the main tectonic processes that took place in the study area of southern Italy with the goal of associating the individual fracture sets to given structural assemblages. Finally, distribution of both P20 and P21 values is considered in order to decipher the fracture stratigraphy of the Mesozoic platform carbonates. Il this regard, we focus on the intensity distribution computed for the most common fracture set pre-dating transtensional faulting.

5.a Depositional Setting

The Apennine Platform is considered as part of the bridge that connected the African Plate to the Adria microplate (Zarcone *et al.*, 2010; Randazzo *et al.*, 2021). The carbonate factory of the Apennine Platform was established in the Late Triassic, and lasted until middle Cretaceous (Sartoni & Crescenti, 1961; Selli, 1957,1962). Previous studies ascribed the study Viggiano Mt. carbonates to the Alburno-Cervati Unit (Lechler *et al.*, 2012), which represented the inner portion of the Apennine Platform.

In the mud-supported bpa, according to microfacies observations, the dark-muddy limestone formed in an inner shallow platform environment (Flugel, 2004). The association between large benthic foraminifera and algae also suggests that carbonate deposition occurred in well oxygenated, warm waters of tropical and subtropical latitudes (Fugagnoli, 2004). Occurrence of carbonate grainstones and packstones with ooids and irregular clasts is interpreted as due to occasional turbulent conditions (Flugel, 2004; Clari 1975). Presence of thick shell of *Lithiotis* bivalves and rare ooids in the aforementioned rocks is therefore consistent with heterogeneous depositional environments also characterized by build-ups and sand shoals (Gale, 2005). Accordingly, we assess that deposition took place in a lagoon protected by sand shoals. The informal litho-biostratigraphic zonation is mainly based on benthic foraminifers and calcareous algae association. It is known that the distribution of the *Palaeodasycladus mediterraneus* ranges throughout the Lower Jurassic (Barattolo, 1991). However, the association of this algae with benthic foraminifera such as *Haurania* sp., *Siphovalvulina* sp., *Lituosepta* sp. is consistent with the mud-supported bpa being upper Sinemurian-Pliensbachian age. The benthic foraminifera association is characterized by larger agglutinated species, which indicates stable and well-oxygenated water conditions, which occurred after the end of the Triassic extinction event (Barattolo and Romano, 2005; Mancinelli *et al.*, 2005; Boudagher Fadel and Bosence, 2007, Todaro *et al.*, 2017).

The oolithic grainstones are also consistent with presence of sand shoals in the depositional environment, indicating high energy conditions above fair-weather wave base (Flugel, 2004). The Lower Jurassic stratigraphy of many western Tethyan carbonate successions shows that carbonate platforms were characterized by a wide low gradient ramp rimmed by sand shoals (Boudager Fadel *et al.*, 2008). Development of the sandy margins was hence a consequence of the absence of sponge reefs (End Triassic Mass Extinction, Di Stefano *et al.*, 1996, Todaro *et al.*, 2018). The lithofacies transition between the mud supported and oolithic bpa's marks a relative deepening of the platform, and the landward migration of the sand shoals. This transition converges with others Lower Jurassic succession of the western Tethys (Ettinger *et al.*, 2021). Formation of the thick oolithic limestones above shallow-water carbonates likely occurred after a major transgression and mass extinction (Mei & Gao, 2012). The results of biostratigraphic analyses point out to a biological turnover between mud supported and oolithic bpa's. The Pliensbachian-Toarcian extinction is associated to a sequence boundary related to a transgression phase (Hallam, 1997; Haq, 2017). This rapid sea level rise determined the drowning of the carbonate platform, with the consequence stillstand of the carbonate factory.

The lithofacies association documented in the breccia bpa is indicative of a high energy shelf environment. In detail, presence of shallow-water biota, rounded skeletal fragments, and/or pristine rudist fossils (*Caprinids* bouquet in growth position, Bentivenga *et al.*, 2017) suggests a depositional setting close to the platform margin (reef to fore-reef) with a moderate to high energy level (Hughes, 2000; Di Stefano & Ruberti, 2000). On the other hand, occurrence of stromatolites, ooids, and oncoids suggests a more internal lagoonal-tidal environment not far from the margin.

A similar depositional environment was described in northern Sicily by Di Stefano & Ruberti (2000), who documented a Cenomanian carbonate platform whose margin included rudist patch reefs in which long-lasting, in situ, wave reworking determined the deposition of poorly sorted rudtsone/floatstone. Moreover, presence of stromatolitic laminae is consistent with a relative sea level oscillation, whereas that of meniscus cements suggests a possible vadose fluid circulation during subaerial exposure of the platform margin (Flugel, 2004).

5.b Diagenetic evolution

The analysis of clay minerals can help to define the paleoclimatic conditions of depositional environments, and to retrieve information on the diagenetic rock evolution by assessing the mineralogical transformations (Hoffman &Hower, 1979; Chamley, 1989; Thiry, 2000; Cavalcante *et al.*, 2003; 2011; Mazzoli *et al.*, 2008; Perri *et al.*, 2012; Garzanti *et al.*, 2014; Tateo, 2020; Hurst *et al.*, 2021; Bitchong *et al.*, 2021; Waliczek *et al.*, 2021). The analysed mixed carbonate terrigenous powder samples deriving from bed package interfaces and surrounding carbonate beds pertaining to the mud-supported bpa include clay minerals. The very low amount, or absence, of goethite, kaolinite, hematite and boemite in the powder samples suggests that the terrigenous component was not involved in post-sedimentary reworking processes and sub-aerial alteration (Agosta *et al.*,2021). The features of mixed layers I/S are consistent with a thermal maturity (130-140 °C) typical of high diagenetic conditions (Merrimman & Peacor, 1999; Cavalcante *et al.*, 2012; Perri *et al.*, 2016; Waliczek *et al.*, 2021). However, since illitization of smectite and formation of mixed-layers not only depends on temperature, but also on the amount of time (McCubbin & Patton, 1981) and K-availability (Cavalcante *et al.*, 2007; 2015; Perri *et al.*, 2012; 2016). Since the study sediments are quite old (Lower Jurassic), it is possible that the temperature was lower than that, corresponding to ca. 100 °C. Taking a geothermal gradient of about 20 °C into account, which is typical of accretionary wedge (Merriman, 2005), a load up to ca. 4-km is estimated. Considering an overall thickness < 1 km of the study platform carbonates, the structural stacking of more internal units of the southern Apennines is assessed as the main controlling factor for the diagenetic evolution of the carbonates.

5.c Diffuse vs. localized fractures

The results of multiscale fracture spacing distribution (cf. Chapter 4.6 above) showed that both N292-300E (JV1 set in Fig. 11) and N206E (JV2 set in Fig. 11) high-angle sets are characterized by exponential best fits (Fig. 12). It is known that exponential best fits characterize fracture sets that formed under a uniform stress distribution (Dershowitz & Einstein, 1988), in which the nucleation process is comparable to a Poissonian process (Cruden, 1977). In other words, the probability that a fracture could enucleate within a given space interval (i.e., within a single carbonate bed) is constant. However, we note that the JV1 set is also characterized by a power law distribution characterized by a fractal dimension D corresponding to the slope of the best fit line (Mandelbrot, 1983). Fracture sets with power law spacing distribution best fits are associated to localized deformation around fault planes or sheared pre-existing structures (Bonnet *et al.*, 2001 and references therein). The double multiscale spacing distribution computed for the JV1 set is therefore consistent multiple stage of formation.

Together with the coeval JV1 fractures (Fig. 11), the JV2 set forms a cross orthogonal system that likely formed due to a local stress state transition mechanism (Bai & Pollard, 2000; Bai *et al.*, 2002). The cross orthogonal fracture system developed during burial diagenesis (Zhang & Spiers, 2005; Aydin *et al.*, 2006; Agosta and Aydin, 2006; Agosta *et al.*, 2009; Lamarche *et al.*, 2012; Lavenu *et al.*, 2014; Agosta *et al.*, 2015; Rustichelli *et al.*, 2015), and/or foreland bulging of the

Apennine Platform (Billi & Salvini, 2003; Tavani *et al.*, 2015).The fracture sets characterized by power law distributions, with D-values comprised between 0.76 and 0.56 (Mandelbrot, 1983), are interpreted as due to localized faulting (Bonnet et al, 2001 and references therein), as assessed for incipient and small faults in the nearby Monte Alpi carbonates by Giuffrida *et al.* (2019, 2020).

5.d Fracture assemblages

According to the existing bibliography, both PSS1a and PSS1b sets likely formed during burial diagenesis, possibly at relatively low values of burial conditions (Dunnington, 1967; Buxton & Sibley, 1981; Tada & Siever, 1981, Agosta *et al.*, 2009; Korneva *et al.*, 2014, Rustichelli *et al*,.2015; Toussaint *et al.,* 2018, Agosta *et al.*, 2021). As shown by their mutual abutting relations with respect to PSS1 (cf. Fig. 11), JV1 veins (E-W to ENE-WSW striking) are also interpreted as due to burial diagenesis. Accordingly, the JV2 (N-S) veins also formed during burial diagenesis. Such a pair relation between bed-parallel PSS and cross-orthogonal bed-perpendicular joints and veins was widely documented in both Apennine and Apulian Platform carbonates of central Italy (Agosta & Aydin 2006; Agosta *et al.* 2010; Aydin *et al.*, 2010; Lavenu *et al.*, 2014), as well as in the Apulian platform carbonates of southern Italy (Korneva *et al.*, 2014; Panza *et al.*, 2016, 2019; Lavenu *et al.*, 2018; Giuffrida *et al.*, 2019; La Bruna *et al.*, 2020). Their coeval formation was hence likely promoted expulsion of the oversaturated fluids from the dissolving zones into the dilating JV1 and JV2 veins (Alvarez *et al.,* 1976; Croizè *et al.* 2010; Gratier *et al.*, 2014; Ben-Itzhak *et al.*, 2014). Altogether, both bed-parallel PSS1a and PSS1b, and both JV1 and JV2 veins hence formed the burial-related structural assemblage (Fig. 13a).

The PSS2 set strikes ca. N-S, and consists of small, sporadic stylolites abutting against PSS1. Although these stylolites are not orthogonal to bedding (ca. 70° cut off angles), we interpret them as due to layer parallel shortening (Nickelsen, 1966, Amrouch *et al.*, 2010), which localized in the paleo carbonate foreland under the effects of a compressive far-field stress and predated the thrusting-related deformation (Holl & Anastasio, 1995). Coeval to the PSS2, we also invoke that bed parallel JV3 veins formed within the carbonates under a similar compressive stress field (Fletcher & Pollard, 1981; Railsback & Andrews, 1995). We also note that some of the pre-existing JV1 (E-W to ENE-WSW striking) were possibly reactivated during layer parallel shortening (Nickelsen, 1966; Ramsay, 1967; Alvarez *et al.*, 1976; Tavani *et al.* 2005). As the thrust front migrated eastward, the Apennine carbonate platform was affected by a large-scale flexure due to foreland bulging (Menardi Noguera & Rea, 2000; Patacca & Scandone, 2007; Vezzani *et al.* 2010). We interpret the JV2 as a re-opened set, due this process, which likely caused formation of dilational fractures parallel to the roughly N-S striking hinge line of the large-scale antiforms (Ramsay, 1967; Billi & Salvini, 2003). Both layer parallel shortening and foreland bulging related fractures are part of the early thrusting structural assemblage (Fig. 13b), which formed during the Burdigalian (layer parallel shortening) and late Burdigalian-Serravallian time intervals, when the outermost thrust front was located westward to the Apennine carbonate platform (Menardi Noguera & Rea, 2000; Patacca & Scandone, 2007; Vezzani *et al.* 2010).

The bed-oblique pressure solution seams PSS3, which dip ca. 70° ENE, are interpreted as due to the thrusting tectonics that involved the study platform carbonates during Serravallian (Menardi Noguera & Rea, 2000; Patacca & Scandone, 2007; Vezzani *et al.* 2010). In particular, we invoke that they formed due to flexural slip deformation that localized within the carbonate multilayer, as suggested by the presence of S-C-C' fabrics within the bed package association interfaces at 4-5 km (cf. Fig. 11). There, the S planes are constituted by pressure solution seams that developed at high angle with respect to the local σ1 principal stress axis (Toussaint *et al.*, 2018, and references therein). In this regard, we note that the individual bed packages were also bounded by clayish interfaces, which could also be affected by localized shear stress and reverse slip. Accordingly, the single carbonate bed packages hence behaved as single mechanical units (Giuffrida *et al.*, 2019) in which the pressure solution processes took place within beds adjacent to the aforementioned interfaces. Both PSS3 and S-C-C' tectonites are hence invoked as part of the thrusting structural assemblage (Fig. 13c), which crosscuts the study Mesozoic platform carbonates. According to the mineralogical data, this structural assemblage developed at depths of ca. 4-5 km, under tectonic load.

The JV4 (NW-SE striking at high angles), JV5 (NE-SW striking at high angles) and both PSS4a and PSS4 b (bot NE-SW striking at low angle) are interpreted as due to the early Pleistocene transtensional tectonics that affected the study area of the High Agri Valley (Cello *et al.*, 1999; Giano *et al.* 2000, Menardi Noguera & Rea, 2000; Patacca & Scandone, 2007; Vezzani *et al.* 2010). Based on the complex cross-cut relations we hypothesize that some JV1 and JV2 structures may have been reactivated. Although we did not observe those, we can infer that both PSS4 sets could have also formed due to transtensional shearing of pre-existing fractures and localized dissolution at their mode II compressive quadrants (Salvini *et al.* 1999; Graham *et al.*, 2003). Altogether, we interpret the JV4, JV5, PSS4a, and PSS4b sets and al the transtensional small faults as part of the transtensional structural assemblage (Fig. 13d).

5.e Fracture Stratigraphy

It is known that fracture density is related to enucleating fracture networks according to the fracture linkage configuration (Myers & Aydin, 2004; Agosta *et al.*, 2006; Demurtas *et al.*, 2016; Mercuri *et al.*, 2020), and to the rock elastic properties (Gross *et al.*, 1995; Agosta *et al.*, 2015; Camanni *et al.*, 2021). Differently, fracture intensity is associated to well-connected fracture networks, which often localize within fault damage zones (Aydin et al 2010; Corradetti et al, 2018; Giuffrida *et al.*, 2019).

In the study Viggiano Mt. area, the P20 and P21 logs show similar trends in both mud supported and oolithic bpa's. High P20 values hence correspond to high P21 values. We note that both P20 and P21 values do not vary proportionally with the bed thickness, as often invoked for layered rock masses (Nur, 1980; Gross *et al.*, 1995; Bai & Pollard, 2000; Schopfer *et al.*, 2011). Differently, both fracture density and intensity computed values are higher for the coarser carbonate beds. This result is also achieved by considering the P10 values computed for the diffuse JV1 set (cf. Table 1). Considering the breccia bpa, the P20 and P21 value do not show similar trends. (cf. Fig. 8b). In fact, the P21 values show a greater variability throughout the stratigraphic succession relative to the P20 values. However, we note that both computed values are commonly higher in correspondence of the coarse-grained carbonate beds.

In light of the aforementioned results, we assess that fracturing was mainly affected by the relative values of the elastic moduli of the carbonates at times of deformation (Wennberg *et al.*, 2006; Larsen *et al.*, 2010). The high P20 and P21 values computed for the coarse-grained carbonates is interpreted as due to their physical and chemical compaction (Rustichelli *et al.* 2012; Rustichelli *et al.*, 2015), and/or cementation (Eberli *et al.* 2003; La Bruna *et al.*, 2020). Accordingly, we invoke that the coarse carbonate beds formed stiff, fractured mechanical units during burial diagenesis and early thrusting, as documented by the P10 values computed for the JV1 set. Further analysis of the cementation processes and micro-fracturing of the study carbonate beds will permit to better assess their diagenetic evolution in relation to development of the micro-fracture network.

Finally, we consider the role exerted by mechanical interfaces (i.e., bed and bed-package interfaces) in the compartmentalization of tensile fractures within specific mechanical units (carbonate beds and bed packages). Both mud-supported and oolithic bpa's show that these interfaces exerted a strong control to the vertical development of the fracture network, as shown by the similar P20 and P21 logs, inhibiting their growth by linkage of pre-existing fractures (Agosta *et al.*, 2015). There, the stress required for vertical fracture growth by linkage was proportional to the mechanical resistance operated by the interfaces (sensu Becker and Gross, 1996). Differently, the breccia bpa did not include efficient mechanical interfaces, as documented in the field. Pronounced bed amalgamation hence allowed the vertical development of the fracture network by linking pre-existing fractures, and strain localization within the evolving fault damage zones. At a larger scale, we note that the Pleinsbachian-Toarcian bed package association interface formed a large-scale mechanical heterogeneity, which controlled strain compartmentalization within the mud-supported and oolithic bpa's. Furthermore, this heterogeneity solved contractional deformation during thrusting tectonics, forming a first order shear zone characterized by a S-C-C'structural fabric

5. Conclusions

In this work, we documented the paleo depositional settings, diagenetic evolution, fracture distribution, main failure modes, structural assemblages, and overall fracture stratigraphy of Mesozoic platform carbonates exposed along the axial zone of the southern Apennines fold and thrust belt, Italy, Basilicata Region. There, three bed packages associations, bpa, respectively labelled as mud supported, oolithic, and breccia were documented according to the carbonate microfacies and fossil associations. The mud supported bpa formed in a low-energy, lagoonal depositional environment during upper Sinemurian-Pliensbachian. There, bed interfaces consisted of bed-parallel pressure solution seams, whereas bed package interfaces included small amounts of terrigenous material. The oolithic bpa is Toarcian in age, formed in high energy conditions above fair-weather wave base within a lagoonal depositional environment. Now days, the oolithic bpa is constituted by amalgamated carbonate beds, and bed package interfaces including thin terrigenous laminae. The aforementioned bpa's are separated by a large-scale stratigraphic interface including 10- to 15 cm-thick mixed carbonate-terrigenous rocks, which marked the Pliensbachian-Toarcian large scale extinction. The breccia bpa formed during Cenomanian, and formed in a lagoonal-tidal environment not far from the platform paleo-margin as shown by presence of stromatolites, ooids, oncoids, and rudist patch reefs. Wave reworking also determined deposition of poorly sorted rudtsones/floatstones. At the present day, the breccia bpa includes coarse-and fine-grained bed alternations characterized by widespread bed amalgamation and bed-parallel pressure solution seams.

Results of quantitative field structural analysis were consistent with presence of five main sets of high-angle fracture throughout the carbonate succession. According to the both P20 and P21 values computed for the layered carbonate succession, primary interfaces such as bed and bed-package interfaces compartmentalized fractures within single mechanical units. Such a behavior was not documented for the breccia bpa, in which the lack of laterally continuous interfaces and pronounced bed amalgamation allowed the vertical fracture development by linkage of pre-existing structural elements. Furthermore, the P10 values computed for the most common, diffuse fracture set, showed that physical-chemical compaction and cementation of the coarse-carbonates took place prior to transtensional faulting throughout the whole carbonate succession. Results of failure modes analysis showed presence of multiple sets of pressure solution seams. Two sets of pervasive, bed-parallel pressure solution seams localized either within the bed interfaces or in the single carbonate beds. Four sets of bed oblique pressure solution seams were documented in the carbonate beds of the mud-supported b.pa. Furthermore, four sets of high angle open fractures and veins, and one set of bed parallel veins were also documented. According to their abutting and crosscutting relations, and also in light of their multi-scale spacing distributions, we associated the formation of specific failure modes to the burial diagenesis, early thrusting, thrusting and transtensional structural assemblages.

Acknowledgements

This work is part of the firs author’s PhD research work. CM acknowledges the help and contribution provided by Grazia de Grazia, Innocenzo Manniello, and Giulia Schirripa Spagnolo during fieldwork. Previous works made by Maria Lechler and Nicola Costantino are deeply acknowledged. The present work is supported by the Reservoir Characterization Project (www.rechproject.com); and by "Geological-Structural and hydrogeologic study of High Agry Valley (Basilicata)” project funded by Eni SpA.

Declaration of interests

The authors declare that they have no known competing financial interests or personal relationships that could have influenced the work reported in this paper.

References

AGOSTA, F. & AYDIN, A. 2006. Architecture and deformation mechanism of a basin-bounding normal fault in Mesozoic platform carbonates, central Italy. *Journal of Structural Geology* **28**(8), 1445–1467.

AGOSTA, F., ALESSANDRONI, M., TONDI, E. & AYDIN, A. 2009. Oblique normal faulting along the northern edge of the Majella Anticline, central Italy: Inferences on hydrocarbon migration and accumulation. *Journal of Structural Geology* **31**(7).

AGOSTA, F., MANNIELLO, C., CAVALCANTE, F., BELVISO C., PROSSER, G., 2021. Late Cretaceous transtensional faulting of the Apulian Platform, Italy. *Marine and Petroleum Geology*. **127**, 104889.

AGOSTA, F., WILSON, C. & AYDIN, A. 2015. The role of mechanical stratigraphy on normal fault growth across a Cretaceous carbonate multi-layer, central Texas (USA). *Italian Journal of Geosciences* **134**(3), 423–441.

ALVAREZ, W., ENGELDER, T. & LOWRIE, W. 1976. Formation of spaced cleavage and folds in brittle limestone by dissolution. *Geology* **4**(11), 698–701.

AMODIO-MORELLI L., BONARDI G., COLONNA V., DIETRICH D., GIUNTA G., IPPOLITO F., LIGUORI V., LORENZONI S., PAGLIONICO A., PERRONE V., PICCARRETA G., RUSSO M., SCANDONE P., ZANETTIN-LORENZONI E. & ZUPPETTA A. (1976). L'Arco calabro-peloritano nell'orogene appenninico-maghrebide. *Mem. Soc. Geol. Ital.*, **17**, 1-60

AMROUCH, K., LACOMBE, O., BELLAHSEN, N., DANIEL, J.M. & CALLOT, J.P. 2010. Stress and strain patterns, kinematics and deformation mechanisms in a basement-cored anticline: Sheep Mountain Anticline, Wyoming. *Tectonics* **29**(1), 1–27.

ANDREO, B., VÍAS, J., DURÁN, J.J., JIMÉNEZ, P., LÓPEZ-GETA, J.A. & CARRASCO, F. 2008. Methodology for groundwater recharge assessment in carbonate aquifers: Application to pilot sites in southern Spain. *Hydrogeology Journal* **16**(5), 911–925.

ANTONELLINI, M., TONDI, E., AGOSTA, F., AYDIN, A. & CELLO, G. 2008. Failure modes in deep-water carbonates and their impact for fault development: Majella Mountain, Central Apennines, Italy. *Marine and Petroleum Geology* **25**(10), 1074–1096.

AYDIN, A. & BERRYMAN, J.G. 2010. Analysis of the growth of strike-slip faults using effective medium theory. *Journal of Structural Geology* **32**(11), 1629–1642.

AYDIN, A., BORJA, R.I. & EICHHUBL, P. 2006. Geological and mathematical framework for failure modes in granular rock. *Journal of Structural Geology* **28**(1), 83–98.

AYDIN, A., ANTONELLINI, M., TONDI, E. & AGOSTA, F. 2010. Deformation along the leading edge of the Maiella thrust sheet in central Italy. *Journal of Structural Geology* **32**(9), 1291–1304.

BAI, T. & POLLARD, D.D. 2000. Fracture spacing in layered rocks: A new explanation based on the stress transition. *Journal of Structural Geology* **22**(1), 43–57.

BAI, T., MAERTEN, L., GROSS, M.R. & AYDIN, A. 2002. Orthogonal cross joints: Do they imply a regional stress rotation? *Journal of Structural Geology* **24**(1), 77–88.

BARATTOLO, F. 1991. Mesozoic and Cenozoic Marine Benthic Calcareous Algae with Particular Regard to Mesozoic Dasycladaleans. In *Calcareous Algae and Stromatolites*, pp. 504–540. , Berlin, Heidelberg: Springer Berlin Heidelberg.

BARATTOLO, F. & ROMANO, R. 2005. Shallow carbonate platform bioevents during the Upper Triassic-Lower Jurassic: An evolutive interpretation. *Bollettino della Societa Geologica Italiana* **124**(1), 123–142.

BECKER, A. & GROSS, M.R. 1996. Mechanism for joint saturation in mechanically layered rocks: An example from southern Israel. *Tectonophysics* **257**(2-4 SPEC. ISS.), 223–237.

BELLANI, S., BROGI, A., LAZZAROTTO, A., LIOTTA, D. & RANALLI, G. 2004. Heat flow, deep temperatures and extensional structures in the Larderello Geothermal Field (Italy): Constraints on geothermal fluid flow. *Journal of Volcanology and Geothermal Research* **132**(1), 15–29.

BENTIVENGA, M., PALLADINO, G., PROSSER, G., GUGLIELMI, P., GEREMIA, F. & LAVIANO, A. 2017. A Geological Itinerary Through the Southern Apennine Thrust Belt (Basilicata—Southern Italy). *Geoheritage* **9**(1), 1–17.

BILLI, A. & SALVINI, F. 2003. Development of systematic joints in response to flexure-related fibre stress in flexed foreland plates: The Apulian forebulge case history, Italy. *Journal of Geodynamics* **36**(4), 523–536.

BITCHONG, A. M., ADATTE, T., NGON NGON, G. F., NGOS III, S. & BILONG, P., 2021. Palynology, mineralogy and geochemistry of sediments in Tondè locality, northern part of Douala sub-basin, Cameroon, Central Africa: implication on paleoenvironment. *Geosciences Journal*, 25, 299-319.

BONNET, E., BOUR, O., ODLING, N.E., DAVY, P., MAIN, I., COWIE, P. & BERKOWITZ, B. 2001. Scaling of fracture systems in geological media. *Reviews of Geophysics* **39**(3), 347–383.

BOUDAGHER-FADEL, M.K. 2008. Chapter 6 The Cenozoic larger benthic foraminifera: the Palaeogene. In *Developments in Palaeontology and Stratigraphy*, pp. 297–545.

BOUDAGHER-FADEL, M.K. & BOSENCE, D.W.J. 2007. Early Jurassic benthic foraminiferal diversification and biozones in shallow-marine carbonates of western Tethys. *Senckenbergiana Lethaea* **87**(1), 1–39.

BRUCE RAILSBACK, L. & ANDREWS, L.M. 1995. Tectonic stylolites in the 'undeformed' Cumberland Plateau of southern Tennessee. *Journal of Structural Geology* **17**(6), 911–915.

LA BRUNA, V., LAMARCHE, J., AGOSTA, F., RUSTICHELLI, A., GIUFFRIDA, A., SALARDON, R. & MARIÉ, L. 2020. Structural diagenesis of shallow platform carbonates: Role of early embrittlement on fracture setting and distribution, case study of Monte Alpi (Southern Apennines, Italy). *Journal of Structural Geology* **131**(June 2019), 103940.

BUTTINELLI, M., IMPROTA, L., BAGH, S. & CHIARABBA, C. 2016. Inversion of inherited thrusts by wastewater injection induced seismicity at the Val d'Agri oilfield (Italy). *Scientific Reports* **6**(November), 1–8.

BUXTON, T.M. & SIBLEY, D.F. 1981. Pressure solution features in a shallow buried limestone. *Journal of Sedimentary Petrology* **51**(1), 19–26.

CAMANNI, G., VINCI, F., TAVANI, S., FERRANDINO, V., MAZZOLI, S., CORRADETTI, A., PARENTE, M. & IANNACE, A. 2021. Fracture density variations within a reservoir-scale normal fault zone: A case study from shallow-water carbonates of southern Italy. *Journal of Structural Geology* **151**(May), 104432.

CASERO P., ROURE F., ENDIGNOUX L., MORETTI I., MÜLLER C., SAGE L. & VIALLY R., 1988. Neogene geodynamic evolution of the Southern Apennines. *Mem. Soc. Geol. Ital.*, **41**, 109-120.

CASERO P., ROURE F. & VIALLY R., 1991. Tectonic framework and petroleum potential of the southern Apennines. In SPENCER A.M. Ed., Generation, accumulation, and production of Europe's hydrocarbons, *Spec. Publ. European Assoc. Petroleum Geosci.*, **1**, 381-387.

CAVALCANTE, F., FIORE, S., PICCARRETA, G., TATEO, F., 2003. Geochemical and mineralogical approaches to assessing provenance and deposition of shales: a case study. *Clay Minerals* **38**, 383–397.

CAVALCANTE, F., FIORE, S., LETTINO, A., PICCARRETA, G. & TATEO, F., 2007. Illite-smectite mixed layers in Sicilide shales and piggy-back deposits of the Gorgoglione Formation (southern Apennines): geological inference. *Boll. Soc. Geol. It*, **126**, 241-254

CAVALCANTE, F., BELVISO, C., BENTIVENGA, M., FIORE, S., PROSSER G., 2011. Occurence of palygorskite and sepiolite in upper Paleocene – middle Eocene marine deep sediments of the Lagonegro basin (Southern Apennines – Italy): paleoenvironmental and provenante inferences. *Sedimentary Geology*, **233**, 42-52.

CAVALCANTE, F., BELVISO, C., LAURITA, S., PROSSER, G., 2012. P-T constraints from phyllosilicates of the Liguride Complex of the Pollino area (Southern Apennines, Italy): Geological inferences. *Ofioliti*, **37**, 65-75.

CELLO, G. & MAZZOLI, S. 1998. Apennine tectonics in southern Italy: A review. *Journal of Geodynamics* **27**(2), 191–211.

CELLO, G., GAMBINI, R., MAZZOLI, S., READ, A., TONDI, E. & ZUCCONI, V. 2000. Fault zone characteristics and scaling properties of the Val d'Agri Fault system (southern Apennines, Italy). *Journal of Geodynamics* **29**(3–5), 293–307.

CELLO, G., TONDI, E., MICARELLI, L. & MATTIONI, L. 2003. Active tectonics and earthquake sources in the epicentral area of the 1857 Basilicata earthquake (southern Italy). *Journal of Geodynamics* **36**(1–2), 37–50.

CHAMLEY, H., 1989. Clay Sedimentology. *Springer-Vergal, Berlin, Heidelberg*. 623 *pp*.

CHIOCCHINI, M.,FARINACCI, A.,MANCINELLI, A.,MOLINARI, V.&POTETTI, M., 1994. Biostratigrafia a foraminiferi, dasicladali e calpionelle delle successioni carbonatiche mesozoiche dell'Appennino centrale (Italia).In: MANCINELLI, A.(ed.)Biostratigrafia dell'Italia centrale. *Studi*

Geologici Camerti, VolumeSpeciale,1994, 9–129

Clari, P. 1975. Caratteristiche sedimentologiche e paleontologiche di alcune sezioni dei Calcari Grigi del Veneto. *Mem. Sc. Geol*., **31**, 1-63

Corniello, A., Ducci, D., Ruggieri, G. & Iorio, M. 2018. Complex groundwater flow circulation in a carbonate aquifer: Mount Massico (Campania Region, Southern Italy). Synergistic hydrogeological understanding. *Journal of Geochemical Exploration* **190**(2017), 253–264.

Corradetti, A., Tavani, S., Parente, M., Iannace, A., Vinci, F., Pirmez, C., Torrieri, S., Giorgioni, M., Pignalosa, A. & Mazzoli, S. 2018. Distribution and arrest of vertical through-going joints in a seismic-scale carbonate platform exposure (Sorrento peninsula, Italy): insights from integrating field survey and digital outcrop model. *Journal of Structural Geology* **108**(September 2017), 121–136.

Croizé, D., Renard, F., Bjørlykke, K. & Dysthe, D.K. 2010. Experimental calcite dissolution under stress: Evolution of grain contact microstructure during pressure solution creep. *Journal of Geophysical Research: Solid Earth* **115**(9), 1–15.

Cruden, D.M. 1977. Describing the size of discontinuities. *International Journal of Rock Mechanics and Mining Sciences and* **14**(3), 133–137.

Cuadros, J. and Altaner, S. P., 1998. Characterization of mixed-layer illite-smectite from bentonites using microscopic, chemical, and X-ray methods: Constraints on the smectite-to-illite transformation mechanism. *American Mineralogist,* **83**, 762–774.

De Castro, P., 1991. Mesozoic. In:Barattolo, F.,De Castro, P.& Parente,M.(eds)*5th International Symposium on Fossil Algae. Field Trip Guide-Book. Giannini*, Napoli, 21–38

Demurtas, M., Fondriest, M., Balsamo, F., Clemenzi, L., Storti, F., Bistacchi, A. & Di Toro, G. 2016.

Structure of a normal seismogenic fault zone in carbonates: The Vado di Corno Fault, Campo Imperatore, Central Apennines (Italy). *Journal of Structural Geology* **90**, 185–206.

DERSHOWITZ, W. S., AND H. H. EINSTEIN, 1988. Characterizing rock joint geometry with joint system models, *Rock Mech. Rock Eng*., **21**, 21-51.

DERSHOWITZ, W.S. & HERDA, H.H. 1992. Interpretation of fracture spacing and intensity. *The 33rd U.S. Symposium on Rock Mechanics (USRMS)*, ARMA-92-0757.

DI NIRO, A., GIANO, S.I., SANTANGELO, N., 1992. Primi dati sull'evoluzione geomorfologica e sedimentaria del bacino dell'alta val d'Agri (Basilicata). *Studi Geologici Camerti* 1992,**1**, 257-263.

DI STEFANO, P., A. ALESSI, AND M. GULLO 1996. Mesozoic and Paleogene megabreccias in southern Sicily: New data on the Triassic paleomarginof the Siculo-Tunisian platform. *Facies*, **34**, 101–122

DOGLIONI, C., HARABAGLIA, P., MARTINELLI, G., MONGELLI, F. & ZITO, G. 1996. A geodynamic model of the Southern Apennines accretionary prism. *Terra Nova* **8**(6), 540–547.

DUNHAM, R.J. 1962. Classification of Carbonate Rocks According to Depositional Texture1 (ed. W. E. Ham). *Classification of Carbonate Rocks—A Symposium* **1**, 0.

DUNNINGTON, H. V 1967. Aspects of Diagenesis and Shape Change in Stylolitic Limestone Reservoirs. *7th World Petroleum Congress*, WPC-12129.

EBERLI, G.P., BAECHLE, G.T., ANSELMETTI, F.S. & INCZE, M.L. 2003. Factors controlling elastic properties in carbonate sediments and rocks. *Leading Edge (Tulsa, OK)* **22**(7), 654–660.

EMBRY, A.F. & KLOVAN, J.E. 1971. A LATE DEVONIAN REEF TRACT ON NORTHEASTERN BANKS ISLAND, N.W.T.1. *Bulletin of Canadian Petroleum Geology* **19**(4), 730–781.

ETTINGER, N.P., LARSON, T.E., KERANS, C., THIBODEAU, A.M., HATTORI, K.E., KACUR, S.M. & MARTINDALE, R.C. 2021. Ocean acidification and photic-zone anoxia at the Toarcian Oceanic Anoxic Event: Insights from the Adriatic Carbonate Platform. *Sedimentology* **68**(1), 63–107.

FLETCHER, R.C. & POLLARD, D.D. 1981. Anticrack model for pressure solution surfaces. *Geology* **9**(9), 419–424.

FLÜGEL, E. 2004. *Microfacies of Carbonate Rocks*.

FU, Y., HAO, Q., PENG, S., MARKOVIC S. B., GAO X., HAN L., WU X., NAMIER, N., ZHANG, W., GAVRILOV, M. B., MARKOVIC, R., GUO, Z., 2021. Clay mineralogy of the Stari Slankamen (Serbia) loess-paleosol sequence during the last glacial cycle d Implications for dust provenance and interglacial climate. *Quaternary Science Reviews,* **263**, 106990

FUGAGNOLI, A. 2004. Trophic regimes of benthic foraminiferal assemblages in Lower Jurassic shallow water carbonates from northeastern Italy (Calcari Grigi, Trento Platform, Venetian Prealps). *Palaeogeography, Palaeoclimatology, Palaeoecology* **205**, 111–130.

GALE, A.S., KENNEDY, W.J., VOIGT, S. & WALASZCZYK, I. 2005. Stratigraphy of the Upper Cenomanian-Lower Turonian Chalk succession at Eastbourne, Sussex, UK: Ammonites, inoceramid bivalves and stable carbon isotopes. *Cretaceous Research* **26**(3), 460–487.

GARZANTI, E., PADOAN, M., SETTI, M., LÓPEZ-GALINDO, A. & VILLA I. M. 2014 Provenance versus weathering control on the composition of tropical river mud (southern Africa). *Chemical Geology*, 366, 61–74.

GIANO, S.I., MASCHIO, L., ALESSIO, M., FERRANTI, L., IMPROTA, S. & SCHIATTARELLA, M. 2000. Radiocarbon dating of active faulting in the Agri high. *Journal of Geodynamics* **29**, 371–386.

GIUFFRIDA, A., LA BRUNA, V., CASTELLUCCIO, P., PANZA, E., RUSTICHELLI, A., TONDI, E., GIORGIONI, M. & AGOSTA,

F. 2019. Fracture simulation parameters of fractured reservoirs: Analogy with outcropping carbonates of the Inner Apulian Platform, southern Italy. *Journal of Structural Geology* **123**, 18–41.

GIUFFRIDA, A., AGOSTA, F., RUSTICHELLI, A., PANZA, E., LA BRUNA, V., ERIKSSON, M., TORRIERI, S. & GIORGIONI, M. 2020. Fracture stratigraphy and DFN modelling of tight carbonates, the case study of the Lower Cretaceous carbonates exposed at the Monte Alpi (Basilicata, Italy). *Marine and Petroleum Geology* **112**(May 2019), 104045.

GRAHAM, B., ANTONELLINI, M. & AYDIN, A. 2003. Formation and growth of normal faults in carbonates within a compressive environment. *Geology* **31**(1), 11–14.

GRATIER, J.P., RENARD, F. & VIAL, B. 2014. Postseismic pressure solution creep: Evidence and time-dependent change from dynamic indenting experiments. *Journal of Geophysical Research: Solid Earth* **119**(4), 2764–2779.

GROSS, M.R. 1993. The origin and spacing of cross joints: examples from the Monterey Formation, Santa Barbara Coastline, California. *Journal of Structural Geology* **15**(6), 737–751.

GROSS, M.R., FISCHER, M.P., ENGELDER, T. & GREENFIELD, R.J. 1995. Factors controlling joint spacing in interbedded sedimentary rocks: Integrating numerical models with field observations from the Monterey Formation, USA. *Geological Society Special Publication* **92**, 215–233.

GROSS, M.R., GUTIÉRREZ-ALONSO, G., BAI, T., WACKER, M.A., COLLINSWORTH, K.B. & BEHL, R.J. 1997. Influence of mechanical stratigraphy and kinematics on fault scaling relations. *Journal of Structural Geology* **19**(2), 171–183.

HIPPOLYTE, J.C., ANGELIER, J. & BARRIER, E. 1995. Compressional and extensional tectonics in an arc system: example of the Southern Apennines. *Journal of Structural Geology* **17**(12), 1725–

1740.

HOFFMAN, J. AND HOWER, J., 1979 Clay mineral assemblages as low grade metamorphic geothermometers: Application to the thrust faulted disturbed belt of Montana: in Aspects of Diagenesis. *P. A. Scholle and P. S. Schluger, eds., SEPM Spec*. Publ. **26**, 55-79.

HOLL, J.E. & ANASTASIO, D.J. 1995. Cleavage development within a foreland fold and thrust belt, southern Pyrenees, Spain. *Journal of Structural Geology* **17**(3), 357–369.

HUGHES, T.P. & TANNER, J.E. 2000. Recruitment Failure, Life Histories, and Long-Term Decline of Caribbean Corals. *Ecology* **81**(8), 2250.

HURST, A., WILSON, M.J., GRIPPA, A., WILSON, L., PALLADINO, G., BELVISO, C., CAVALCANTE, F., 2021. Provenance and Sedimentary Context of Clay Mineralogy in an Evolving Forearc Basin, Upper Cretaceous-Paleogene and Eocene Mudstones, San Joaquin Valley, California. *Minerals*, 11, 71.

IMPROTA L., IANNACCONE G., CAPUANO P., ZOLLO A. & SCANDONE P., 2000. Inferences on the upper crustal structure of Southern Apennines (Italy) from seismic refraction investigations and subsurface data. *Tectonophysics*, **317** (3-4), 273-297.

KASTENS, K. & MASCLE, J. 1990. The geological evolution of the Tyrrhenian Sea: an introduction to the scientific results of ODP Leg 107. *Proc., scientific results, ODP, Leg 107, Tyrrhenian Sea* **107**(1986), 3–26.

KORNEVA, I., TONDI, E., AGOSTA, F., RUSTICHELLI, A., SPINA, V., BITONTE, R. & DI CUIA, R. 2014. Structural properties of fractured and faulted Cretaceous platform carbonates, Murge Plateau (southern Italy). *Marine and Petroleum Geology* **57**, 312–326.

LAMARCHE, J., LAVENU, A.P.C., GAUTHIER, B.D.M., GUGLIELMI, Y. & JAYET, O. 2012. Relationships between fracture patterns, geodynamics and mechanical stratigraphy in Carbonates (South-East Basin, France). *Tectonophysics* **581**, 231–245.

Laronne Ben-Itzhak, L., Aharonov, E., Karcz, Z., Kaduri, M. & Toussaint, R. 2014. Sedimentary stylolite networks and connectivity in limestone: Large-scale field observations and implications for structure evolution. *Journal of Structural Geology* **63**, 106–123.

Larsen, B., Gudmundsson, A., Grunnaleite, I., Sælen, G., Talbot, M.R. & Buckley, S.J. 2010. Effects of sedimentary interfaces on fracture pattern, linkage, and cluster formation in peritidal carbonate rocks. *Marine and Petroleum Geology* **27**(7), 1531–1550.

Laubach, S.E., Olson, J.E. & Cross, M.R. 2009. Mechanical and fracture stratigraphy. *AAPG Bulletin* **93**(11), 1413–1426.

Lavenu, A.P.C. & Lamarche, J. 2018. What controls diffuse fractures in platform carbonates? Insights from Provence (France) and Apulia (Italy). *Journal of Structural Geology* **108**, 94–107.

Lavenu, A.P.C., Lamarche, J., Salardon, R., Gallois, A., Marié, L. & Gauthier, B.D.M. 2014. Relating background fractures to diagenesis and rock physical properties in a platform-slope transect. Example of the Maiella Mountain (central Italy). *Marine and Petroleum Geology* **51**, 2–19.

M Lechler, G Frijia, M Mutti, G Palladino, G Prosser (2012) - Stratigraphic setting of a segment from the Eastern margin of the Apennine platform (Monte di Viggiano, Southern Apennines). *Rendiconti Online S.G.I.*, **21**, 1012-1013.

Lucia, F.J. 1983. Petrophysical Parameters Estimated From Visual Descriptions of Carbonate Rocks: a Field Classification of Carbonate Pore Space. *JPT, Journal of Petroleum Technology* **35**(3), 629–637.

Lucia, F.J. & Fogg, G.E. 1990. Geologic/stochastic mapping of heterogeneity in a carbonate reservoir. *JPT, Journal of Petroleum Technology* **42**(10), 1298–1303.

M. B. Rohrbaugh Jr., 1 W. M. Du 2002. Estimating fracture trace intensity, density, and mean length using circular scan lines and windows. *AAPG Bulletin* **86**.

Malinverno, A. & Ryan, W.B.F. 1986. Extension in the Tyrrhenian Sea and shortening in the Apennines as result of arc migration driven by sinking of the lithosphere. *Tectonics* **5**(2), 227–245.

Mallet R., 1862. Great Neapolitan Earthquake of 1857. The First Principles of Observational Seismology. *London*, 2 voll.

Mancinelli, A., Chiocchini, M., Chiocchini, R.A. & Romano, A. 2005. Biostratigraphy of Upper Triassic-Lower Jurassic carbonate platform sediments of the central-southern Apennines (Italy). *Rivista Italiana di Paleontologia e Stratigrafia* **111**(2), 271–283.

Mandelbrot, B.B. & Wheeler, J.A. 1983.The Fractal Geometry of Nature. *American Journal of Physics* **51**(3), 286–287.

Marín, A.I. & Andreo, B. 2015. *Vulnerability to Contamination of Karst Aquifers*, 251–266p.

Maschio, L., Ferranti, L. & Burrato, P. 2005. Active extension in Val d'Agri area, southern Apennines, Italy: Implications for the geometry of the seismogenic belt. *Geophysical Journal International* **162**(2), 591–609.

Mauldon, M., Dunne, W.M. & Rohrbaugh, M.B. 2001. Circular scanlines and circular windows: New tools for characterizing the geometry of fracture traces. *Journal of Structural Geology* **23**(2–3), 247–258.

Mazzoli, S., D'Errico, M., Aldega, L.,Corrado S., Invernizzi C., Shiner P. & Zattin M., 2008. Tectonic burial and "young" (<10 Ma) exhumation in the southern Apennines fold-and-thrust belt

(Italy). *Geology*, **36**, 243-246.

McCubbin, D. G. and Patton, J.W., 1981. Burial diagenesis of illite/smectite: The kinetic model*:* *Amer. Assoc. Petrol. Geol. Bull.* **65**, 956.

Mei, M. & Gao, J. 2012. Giant Induan oolite: A case study from the Lower Triassic Daye Formation in the western Hubei Province, South China. *Geoscience Frontiers* **3**(6), 843–851.

Mercuri, M., Carminati, E., Tartarello, M.C., Brandano, M., Mazzanti, P., Brunetti, A., McCaffrey, K.J.W. & Collettini, C. 2020. Lithological and structural control on fracture frequency distribution within a carbonate-hosted relay ramp. *Journal of Structural Geology* **137**(May).

Merriman, R.J., 2005. Clay minerals and sedimentary basin history. *European Journal of Mineralogy*, **17**, 7-20.

Monaco C., Tortorici L. & Paltrinieri W., 1998. Structural evolution of the Lucanian Apennines, southern Italy. *Journ. Struct. Geol.*, **20**, 617-638.

Moore, D.M. & Reynolds, R.C., Jr., 1997. X-ray Diffraction and Identification and Analysis of Clay Minerals, 2nd ed. *Oxford University Press: Oxford, UK; New York, NY, USA*, 378p.

Moore, C.H. 2002. Carbonate Reservoirs Porosity Evolution and Diagenesis in a Sequence Stratigraphic Framework. *Marine and Petroleum Geology* **19**(10), 1295–1296.

Mosca, F., Wavrek, D. A., 2002. Petroleum System Characteristics Of Val D'Agri Region, Southern Apennines, Italy. In: *AAPG Annual Conference And Exhibition (Abstract Book)*.

Mostardini F. & Merlini S. 1986. Appennino centro-meridionale. Sezioni geologiche e proposta di modello strutturale. *Mem. Soc. Geol. Ital.*, **35**, 177-202.

Myers, R. & Aydin, A. 2004. The evolution of faults formed by shearing across joint zones in sandstone. *Journal of Structural Geology* **26**(5), 947–966.

NICKELSEN, R.P. 1966. Fossil Distortion and Penetrative Rock Deformation in the Appalachian Plateau, Pennsylvania. *The Journal of Geology* **74**(6), 924–931.

NOGUERA, A.M. & REA, G. 2000. Deep structure of the Campanian-Lucanian Arc (Southern Apennine, Italy). *Tectonophysics* **324**(4), 239–265.

NOVELLINO, R., PROSSER, G., SPIESS, R., VITI, C., AGOSTA, F., TAVARNELLI, E. & BUCCI, F. 2015. Dynamic weakening along incipient low-angle normal faults in pelagic limestones (Southern Apennines, Italy). *Journal of the Geological Society* **172**(February), 283–286.

NUR, A. & ISRAEL, M. 1980. The role of heterogeneities in faulting. *Physics of the Earth and Planetary Interiors* **21**(2–3), 225–236.

ODLING, N.E., GILLESPIE, P., BOURGINE, B., CASTAING, C., CHILÉS, J.P., CHRISTENSEN, N.P., FILLION, E., GENTER, A., OLSEN, C., THRANE, L., TRICE, R., AARSETH, E., WALSH, J.J. & WATTERSON, J. 1999. Variations in fracture system geometry and their implications for fluid flow in fractured hydrocarbon reservoirs. *Petroleum Geoscience* **5**(4), 373–384.

PANZA, E., AGOSTA, F., RUSTICHELLI, A., ZAMBRANO, M., TONDI, E., PROSSER, G., GIORGIONI, M. & JANISECK, J.M. 2016. Fracture stratigraphy and fluid flow properties of shallow-water, tight carbonates: The case study of the Murge Plateau (southern Italy). *Marine and Petroleum Geology* **73**, 350–370.

PANZA, E., AGOSTA, F., RUSTICHELLI, A., VINCIGUERRA, S.C., OUGIER-SIMONIN, A., DOBBS, M. & PROSSER, G. 2019. Meso-to-microscale fracture porosity in tight limestones, results of an integrated field and laboratory study. *Marine and Petroleum Geology* **103**(November 2018), 581–595.

PATACCA E., SARTORI R. & SCANDONE P., 1990. Tyrrhenian basin and Apenninic arcs: kinematic relations since Late Tortonian times*. Mem. Soc. Geol. Ital.*, **45**, 425-451.

PATACCA E., SCANDONE P., BELLATALLA M., PERILLI N. & SANTINI U. 1992°. The Numidian-sand event in the Southern Apennines. Mem. Sci. Geol. già Mem. Ist. Geol. Mineral. Univ. Padova, all. **43**, 297-337.

PATACCA E., SCANDONE P., BELLATALLA M., PERILLI N. & SANTINI U., 1992b. La zona di giunzione tra l'arco appenninico settentrionale e l'arco appenninico meridionale nell'Abruzzo e nel Molise. In: TOZZI M., CAVINATO G.P. & PAROTTO M. Eds., «Studi preliminari all'acquisizione dati del profilo CROP 11 Civitavecchia-Vasto», AGIP-CNR-ENEL. *Studi Geol. Camerti, Vol. Spec. 1991-* **2**, 417-441.

PATACCA, E. & SCANDONE, P. 2007. Geology of the Southern Apennines. *Bollettino della Societa Geologica Italiana, Supplemento* **7**(October), 75–119.

PETRELLA, E., AQUINO, D., FIORILLO, F. & CELICO, F. 2015. The effect of low-permeability fault zones on groundwater flow in a compartmentalized system. Experimental evidence from a carbonate aquifer (Southern Italy). *Hydrological Processes* **29**(6), 1577–1587.

PERRI, F., CRITELLI, S., CAVALCANTE, F., MONGELLI, G., DOMINICI, R., SONNINO, M., DE ROSA, R., 2012. Provenance signatures for the Miocene volcaniclastic succession of the Tufiti di Tusa Formation, southern Apennines, Italy.*Geol. Mag.***149**, 423–442.

PERRI, F., CARACCIOLO, L., CAVALCANTE, F., CORRADO, S.; CRITELLI, S., MUTO, F., DOMINICI, R., 2016. Sedimentary and thermal evolution of the Eocene-Oligocene mudrocks from the southwestern Thrace Basin (NE Greece). Basin Res. 28, 319–339.

PIEDILATO, S., PROSSER, G. 2005. Thrust sequences and evolution of the external sector of a fold and thrust belt: An example from the Southern Apennines (Italy). *Journal of Geodynamics* **39**, 386–402.

POLLARD, D.D. & AYDIN, A. 1990. Progress in understanding jointing over the past century. *Special Paper of the Geological Society of America* **253**, 313–336.

RAMSAY, J. G. 1967. Folding and fracturing of rocks. *Mc Graw Hill Book Company*, 568.

RUSTICHELLI, A., TONDI, E., AGOSTA, F., CILONA, A. & GIORGIONI, M. 2012. Development and distribution of bed-parallel compaction bands and pressure solution seams in carbonates (Bolognano Formation, Majella Mountain, Italy). *Journal of Structural Geology* **37**, 181–199.

RUSTICHELLI, A., TONDI, E., KORNEVA, I., BAUD, P., VINCIGUERRA, S., AGOSTA, F., REUSCHLÉ, T. & JANISECK, J.M. 2015. Bedding-parallel stylolites in shallow-water limestone successions of the Apulian carbonate platform (central-Southern Italy). *Italian Journal of Geosciences* **134**(3), 513–534.

SALVINI, F., BILLI, A. & WISE, D.U. 1999. Strike-slip fault-propagation cleavage in carbonate rocks: The Mattinata Fault zone, southern Apennines, Italy. *Journal of Structural Geology* **21**(12), 1731–1749.

SARTONI S. & CRESCENTI U. 1961. Ricerche biostratigrafiche nel Mesozoico dell'Appennino meridionale. *G. Geol.*, s. 2, **29**, 161- 302.

SCHETTINO, A. & TURCO, E. 2011. Tectonic history of the Western Tethys since the Late Triassic. *Bulletin of the Geological Society of America* **123**(1–2), 89–105.

SCHÖPFER, M.P.J., ARSLAN, A., WALSH, J.J. & CHILDS, C. 2011. Reconciliation of contrasting theories for fracture spacing in layered rocks. *Journal of Structural Geology* **33**(4), 551–565.

SCROCCA, D., CARMINATI, E. & DOGLIONI, C. 2005. Deep structure of the southern Apennines, Italy: Thin-skinned or thick-skinned? *Tectonics* **24**(3), 1–20.

SELLI R., 1957. Sulla trasgressione del Miocene nell'Italia meridionale, *G. Geol.*, s. 2, **26**, 1-54.

SELLI R., 1962. Il Paleogene nel quadro della geologia dell'Italia Meridionale, *Mem. Soc. Geol. Ital.*,

3, 733-7

SHINER, P., BECCACINI, A. & MAZZOLI, S. 2004. Thin-skinned versus thick-skinned structural models for Apulian carbonate reservoirs: Constraints from the Val d'Agri Fields, S Apennines, Italy. *Marine and Petroleum Geology* **21**(7), 805–827.

SMERAGLIA, L., GIUFFRIDA, A., GRIMALDI, S., PULLEN, A., LA BRUNA, V., BILLI, A. & AGOSTA, F. 2021. Fault-controlled upwelling of low-T hydrothermal fluids tracked by travertines in a fold-and-thrust belt, Monte Alpi, southern apennines, Italy. *Journal of Structural Geology* **144**(December 2020), 104276.

SPALLUTO, L. 2008. Sedimentology and high -resolution sequence stratigraphy of a Lower Cretaceous shallow-water carbonate succession from the western Gargano Promontory (Apulia, Southern Italy). *GeoActa, Spec. Publ.* **1**(1991), 77–96.

SPALLUTO, L. 2012. Facies evolution and sequence chronostratigraphy of a 'mid'-Cretaceous shallow-water carbonate succession of the Apulia Carbonate Platform from the northern Murge area (Apulia, southern Italy). *Facies* **58**(1), 17–36.

DI STEFANO, P. & RUBERTI, D. 2000. Cenomanian rudist-dominated shelf-margin limestones from the panormide carbonate platform (Sicily, Italy): Facies analysis and sequence stratigraphy. *Facies* **42**(1), 133–160.

TADA, R. & SIEVER, R. 1989. Pressure solution during diagenesis. *Annual review of earth and planetary sciences. Vol. 17*, 89–118.

TATEO, F., 2020.. Clay Minerals at the Paleocene–Eocene Thermal Maximum: Interpretations, Limits, and Perspectives. *Minerals*, **10**, 1073.

TAVANI, S., STORTI, F., LACOMBE, O., CORRADETTI, A., MUÑOZ, J.A. & MAZZOLI, S. 2015. A review of deformation pattern templates in foreland basin systems and fold-and-thrust belts: Implications for the state of stress in the frontal regions of thrust wedges. *Earth-Science Reviews* **141**, 82–104.

THIRY, M., 2000.. Palaeoclimatic interpretation of clay minerals inmarine deposits: an outlook from the continental origin. *Earth Sci. Rev.* **49**, 201–221.

TODARO, S., DI STEFANO, P., ZARCONE, G. & RANDAZZO, V. 2017. Facies stacking and extinctions across the Triassic–Jurassic boundary in a peritidal succession from western Sicily. *Facies* **63**(3), 1–21.

TODARO, S., RIGO, M., RANDAZZO, V. & DI STEFANO, P. 2018. The end-Triassic mass extinction: A new correlation between extinction events and δ13C fluctuations from a Triassic-Jurassic peritidal succession in western Sicily. *Sedimentary Geology* **368**, 105–113.

TOUSSAINT, R., AHARONOV, E., KOEHN, D., GRATIER, J.P., EBNER, M., BAUD, P., ROLLAND, A. & RENARD, F. 2018. Stylolites: A review. *Journal of Structural Geology* **114**(May), 163–195.

TUCKER, M.E. 1985. Shallow-marine carbonate facies and facies models. *Sedimentology: recent developments and applied aspects* (January 1985), 147–169.

VEZZANI, L., FESTA, A. & GHISETTI, F.C. 2010. Geology and tectonic evolution of the Central-Southern Apennines, Italy. *Special Paper of the Geological Society of America* **469**(January), 1–58.

WALICZEK, M., MACHOWSKI, G., POPRAWA, P., ŚWIERCZEWSKA, A. & WIĘCŁAW D., 2021.. A novel VRo, T*max*, and S indices conversion formulae on data from the fold-and-thrust belt of the Western Outer Carpathians (Poland). *International Journal of Coal Geology*, **234**, 103672.

WENNBERG, O.P., SVÅNÅ, T., AZIZZADEH, M., AQRAWI, A.M.M., BROCKBANK, P., LYSLO, K.B. & OGILVIE, S. 2006. Fracture intensity vs. mechanical stratigraphy in platform top carbonates: The

Aquitanian of the Asmari Formation, Khaviz Anticline, Zagros, SW Iran. *Petroleum Geoscience* **12**(3), 235–245.

WU, H. & D. POLLARD, D. 1995. An experimental study of the relationship between joint spacing and layer thickness. *Journal of Structural Geology* **17**(6), 887–905.

ZARCONE, G., PETTI, F.M., CILLARI, A., DI STEFANO, P., GUZZETTA, D. & NICOSIA, U. 2010. A possible bridge between Adria and Africa: New palaeobiogeographic and stratigraphic constraints on the Mesozoic palaeogeography of the Central Mediterranean area. *Earth-Science Reviews* **103**(3–4), 154–162.

ZHANG, X. & SPIERS, C.J. 2005. Compaction of granular calcite by pressure solution at room temperature and effects of pore fluid chemistry. *International Journal of Rock Mechanics and Mining Sciences* **42**(7-8 SPEC. ISS.), 950–960.

Figure Captions

Figure 1 – (Colour online) a) Simplified structural map of the southern Apennines fold-and-thrust belt, Italy (modified after Piedilato & Prosser , 2005); b) geological map of the High Agri Valley, southern Italy. The white square represents the location of the study Viggiano Mt. area; c) geological cross-section of the Southern Apennines along the A-A' transect (modified after Prosser *et al.,* 2021)

Figure 2 – (Colour online) a) Geological map of the Viggiano Mt. area lying along the northern edge of the High Agri Valley (Palladino et al, pers. comm.). Location of both "Scarrone la Macchia" and "Il Monte" study sites is reported; b, c) schematic stratigraphic logs of: "Scarrone la Macchia", and "Il Monte" areas (modified after Lechler et al., 2012), respectively.

Figure 3 – (Colour online) a) Panoramic view of the "Scarrone la Macchia" site. Bedding surfaces (yellow lines), bed packages surface interfaces (orange lines), and bed packages association surfaces (magenta line) are reported; b) detailed stratigraphic log of the "Scarrone la Macchia" site. Bed packages surfaces (orange lines) and bed packages association surface (dashed magenta line) are highlighted; c) lower-hemisphere, equal-area stereographic projection of the bedding of the two bed packages associations: mud-supported bed package association and oolithic bed package association; d) panoramic view of the "Il Monte" site. Bedding surfaces (yellow dashed lines), bed packages surfaces (orange lines) and bed packages association surface (magenta line) are highlighted; e) stratigraphic section of "Il Monte" site. Bed packages surfaces (dashed orange lines) and bed packages association surface (dashed magenta line) are highlighted; f) lower-hemisphere, equal-area stereographic projection of the bedding of the breccia bed packages association.

Figure 4 – (Colour online) Microfacies of the Scarrone la Macchia section (a-e: mud-supported bpa, f-h: oolithic bpa). a) Packstone with *Thaumatoporella parvovesiculifera.* b) grainstone-packstone woth *Siphovalvulina* sp.; c) grainstone-pakstone with benthic foraminifera (Siphovalvulina sp., *Haurania deserta*, *Lituosepta* sp.); d) *Palaeodasycladus mediterraneus*; e) *Bacinella-Lithocodium* agregatum; f) oolithic grainstone; g) ppen fractures partially occluded by dolomitic cements; h) intergranular porosity.

Figure 5 – (Colour online) Microfacies of the Il Monte section. a), b) and c) grainstone to rudstone with fragments of rudists shell, orbitolinids. d) stromatolitic laminae with peloids. e) meniscus cements connecting the grains and isopacous cements rims around the rudists fragments. Barren silt filled the residual cavities. f) meniscus cements connecting the grains. The residual cavity is filled by a silt reach in ostracods.

Figure 6 – (Colour online) Representative XRD patterns of selected samples. [a] bulk samples and [b] terrigenous components. Cal=calcite, Qtz=quartz, Fs=feldspars, Gt=goethite, Ill=illite, I/S= mixed layers illite/smectite, Chl=chlorite, Kao=kaolinite; Σ Clay minerals= sum clay minerals.

Figure 7 – (Colour online) Representative XRD patterns of ethylene glycol solvated clay fraction powders of selected samples. On the left (a, b, c, d) decomposition at low angles; on the right (a', b', c', d') decomposition at higher angles. Ill=illite, I/S= mixed layers illite/smectite, Chl=chlorite.

Figure 8 – (Colour online) Fracture density (P20) and intensity (P21) logs after field circular scanline measurements conducted across the: a) mud-supported bed package and oolithic bed package associations, and b) breccia bed package association.

Figure 9 – (Colour online) Lower-hemisphere, equal-area stereographic projection of fracture poles after field measurements (left) and after bedding restoration (right). Fracture data restored considering the attitude of single beds from which data were gathered.

Figure 10 - (Colour online) Lower-hemisphere equal-area stereographic projection of fracture poles after field measurements (left) and after bedding restoration (right): a) mud-supported bed packages association dataset; b) oolithic bed packages association dataset; c) breccia bed packages association dataset.

Figure 11 – (Colour online) a) Bed-parallel pressure solution seams (PSS1a and PSS1b), open fractures(JV2) and high angle (PSS2): the PSS1a (blue lines) are laterally continuous and define the actual bedding; PSS1b are bed-internal and have a length of 10s of cm (yellow lines); JV2 (magenta lines) are high angle open fractures that compartmentalize among PSS1a and PSS1b; PSS2 (green lines) are roughly parallel to JV2, have a length <10 cm and compartmentalize mostly among PSS1a and PSS1b. The inset shows the not-interpreted image. b) bed-oblique pressure solution seams PSS3(blue) and PSS4b (magenta) and their cross-cut relation with PSS1b (blue lines); c) bed-perpendicular veins (JV1, blue line) and their cross-cut relation with the PSS1b (yellow lines) and PSS1a (Light-blue bold line); d) bed-parallel veins, JV3 (red arrows), high angle veins JV1 (blue arrows), PSS3 (blue lines), PSS4a (orange lines) and PSS4b (magenta lines). The JV3 veins abut against the JV1 and against PSS. PSS4a and PSS4b abut against PSS3; e) Cross-cut and abutting relations among JV1 (blue lines), JV2(yellow lines), JV4 (red lines) and JV5 (green lines). f) S-C-C' tectonite fabric within a bed package interface. A top-to-NE sense of shear is highlighted.

Figure 12 – (Colour online) Multi-scale fracture spacing distribution. a) Geological map of the area with the location of studied outcrops; b) lower-hemisphere, equal-area stereographic projection of fracture poles of the S1 scan line; c) log cumulative number vs spacing and

best fit relative to the N292 striking set; d) log cumulative number vs spacing and best fit relative to the N300 striking set; e) lower-hemisphere, equal-area stereographic projection of fracture poles of the S2 scan line; f) log cumulative number vs spacing and best fit relative to the N252 striking set; g) log cumulative number vs spacing and best fit relative to the N284 striking set; h) lower-hemisphere, equal-area stereographic projection of fracture poles of the S3 scan line; i) log cumulative number vs spacing and best fit relative to the N180 striking set; l) log cumulative number vs spacing and best fit relative to the N206 striking set.

Figure 13 – (Colour online) Structural assemblages through time: a) burial diagenesis assemblage; b) early thrusting assemblage; c) thrusting assemblage; d) transtensional assemblage.

Table 1. Sample code, litology, components and fractions determined by XRPD on samples collected from the "Scarrone la Macchia" stratigraphic section. n.d.: not detected because is present in very little amount.

Table 2 Mineralogical assemblages of the study samples. Cal: calcite; Qtz: quartz; Fs: feldspars; Gth: goethite; I/S: mixed layers illite-smectite; Ill: illite; Chl: chlorite; Kao: kaolinite. X: indicates the presence of mineral phase; n.d.: not detected.

Table 3. P10 variations for the JV1 fracture set.

Sample	Litology	Random powder of Bulk sample	Rondom powder of terrigenous component	Oriented specimens (< 2 µm fraction) of the terrigenous component
O-2	cohesive limestone	X	n.d.	n.d.
SC1	interbed with terrigenous component	X	X	X
SC2	interbed with terrigenous component	X	X	X
MC1	cohesive limestone	X	X	X
MC3	cohesive limestone	X	X	n.d.
SL2B-C1	interbed with terrigenous component	X	X	X
SL2B-C2	interbed with terrigenous component	X	X	X
MC4	cohesive limestone	X	X	X
SC3	interbed with terrigenous component	X	X	X
MC5	cohesive limestone	X	n.d.	n.d.
MC6	cohesive limestone	X	X	X
SC4	interbed with terrigenous component	X	X	X
MC7	cohesive limestone	X	X	X
A7	cohesive limestone	X	X	n.d.
SC5	interbed with terrigenous component	X	X	X
C1	cohesive limestone	X	X	n.d.
D5	cohesive limestone	X	X	n.d.
D4	cohesive limestone	X	X	n.d.
SC6	interbed with terrigenous component	X	X	X
D2	cohesive limestone	X	X	X

Table 1

Lithofacies	Bed thickness	P10
Grainstone	60 cm	1.79
Grainstone	70 cm	1.26
Wakestone	25 cm	0.85
Wackestone	54 cm	0.3
Grainstone	25 cm	0.86
Oolithic grainstone	55 cm	1.06
Oolithic grainstone	90 cm	0.74
Carbonate breccia	30 cm	1.35
Carbonate breccia	120 cm	0.95
Carbonate breccia	100 cm	0.46

Table 2

Sample	Random powder analysis of bulk sample and terrigenous component								Oriented specimens (< 2µm)			
	Cal	Qtz	Fs	Gth	I/S	Ill	Chl	Kao	I/S features			
									Ordering, R		Illite percentage	
O-2	X	n.d.	n.d.	n.d.	n.d.	n.d.	n.d.	n.d.	n.d.	n.d.	n.d.	n.d.
SC1	X	n.d.	X	n.d.	X	X	X	n.d.	R1	R3	82	89
SC2	X	n.d.	X	n.d.	X	X	X	n.d.	n.d.	R3	n.d.	87
MC1	X	n.d.	X	n.d.	X	X	X	n.d.	n.d.	R3	n.d.	87
MC3	X	X	X	n.d.	X	X	X	n.d.	n.d.	n.d.	n.d.	n.d.
SL2B-C1	X	X	X	n.d.	X	X	X	n.d.	R1	R3	80	90
SL2B-C2	X	X	X	n.d.	X	X	X	n.d.	R1	R3	78	90
MC4	X	X	X	n.d.	X	X	X	n.d.	n.d.	R3	n.d.	87
SC3	X	n.d.	X	n.d.	X	X	X	X	n.d.	R3	n.d.	86
MC5	X	X	n.d.	n.d.	n.d.	n.d.	n.d.	n.d.	n.d.	n.d.	n.d.	n.d.
MC6	X	X	X	n.d.	X	X	X	X	R1	R3	82	89
SC4	X	n.d.	X	X	X	X	X	n.d.	R1	R3	80	89
MC7	X	X	X	X	X	X	X	n.d.	n.d.	R3	n.d.	85
A7	X	X	X	n.d.	X	X	X	n.d.	n.d.	n.d.	n.d.	n.d.
SC5	X	n.d.	X	X	X	X	X	n.d.	n.d.	n.d.	n.d.	n.d.
C1	X	n.d.	X	n.d.	X	X	X	n.d.	n.d.	n.d.	n.d.	n.d.
D5	X	X	X	n.d.	X	X	X	n.d.	n.d.	n.d.	n.d.	n.d.
D4	X	X	X	n.d.	X	X	X	n.d.	n.d.	n.d.	n.d.	n.d.
SC6	X	X	X	X	X	X	X	n.d.	n.d.	R3	n.d.	86
D2	X	n.d.	X	n.d.	X	X	X	n.d.	n.d.	R3	n.d.	87

Table 3

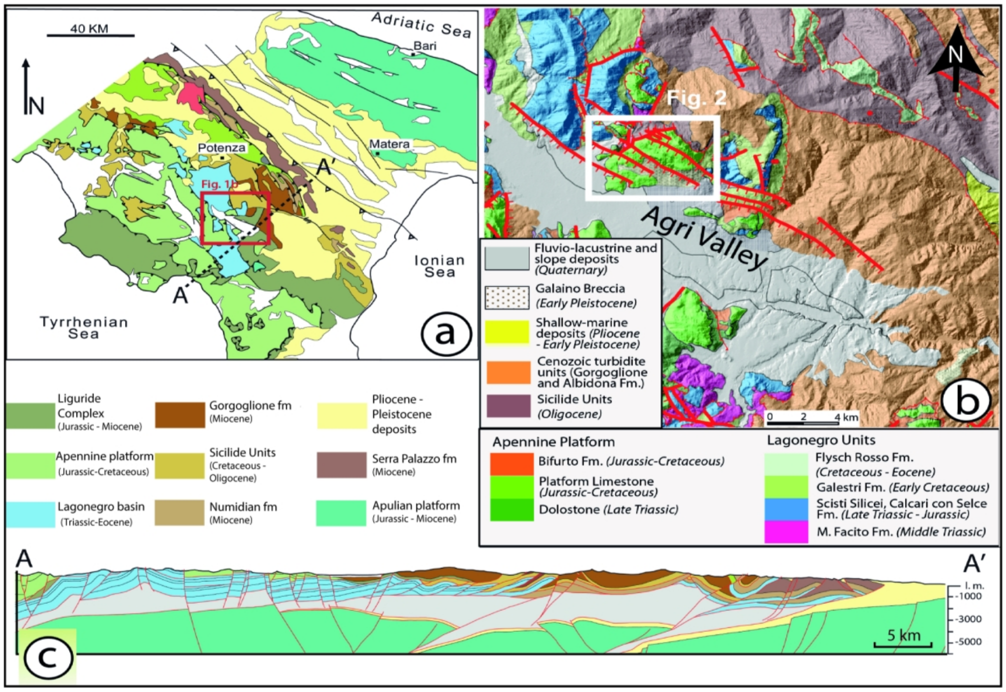

40 KM
Adriatic Sea
Bari
N
Potenza
Matera
A'
Fig. 1b
Ionian Sea
A
Tyrrhenian Sea
a
Fig. 2
Agri Valley
N
b
0 2 4 km
Fluvio-lacustrine and slope deposits (Quaternary)
Galaino Breccia (Early Pleistocene)
Shallow-marine deposits (Pliocene - Early Pleistocene)
Cenozoic turbidite units (Gorgoglione and Albidona Fm.)
Sicilide Units (Oligocene)
Liguride Complex (Jurassic - Miocene)
Gorgoglione fm (Miocene)
Pliocene - Pleistocene deposits
Apennine platform (Jurassic-Cretaceous)
Sicilide Units (Cretaceous - Oligocene)
Serra Palazzo fm (Miocene)
Lagonegro basin (Triassic-Eocene)
Numidian fm (Miocene)
Apulian platform (Jurassic - Miocene)
Apennine Platform
Bifurto Fm. (Jurassic-Cretaceous)
Platform Limestone (Jurassic-Cretaceous)
Dolostone (Late Triassic)
Lagonegro Units
Flysch Rosso Fm. (Cretaceous - Eocene)
Galestri Fm. (Early Cretaceous)
Scisti Silicei, Calcari con Selce Fm. (Late Triassic - Jurassic)
M. Facito Fm. (Middle Triassic)
A
A'
l. m.
-1000
-3000
-5000
5 km
c

Figure 1

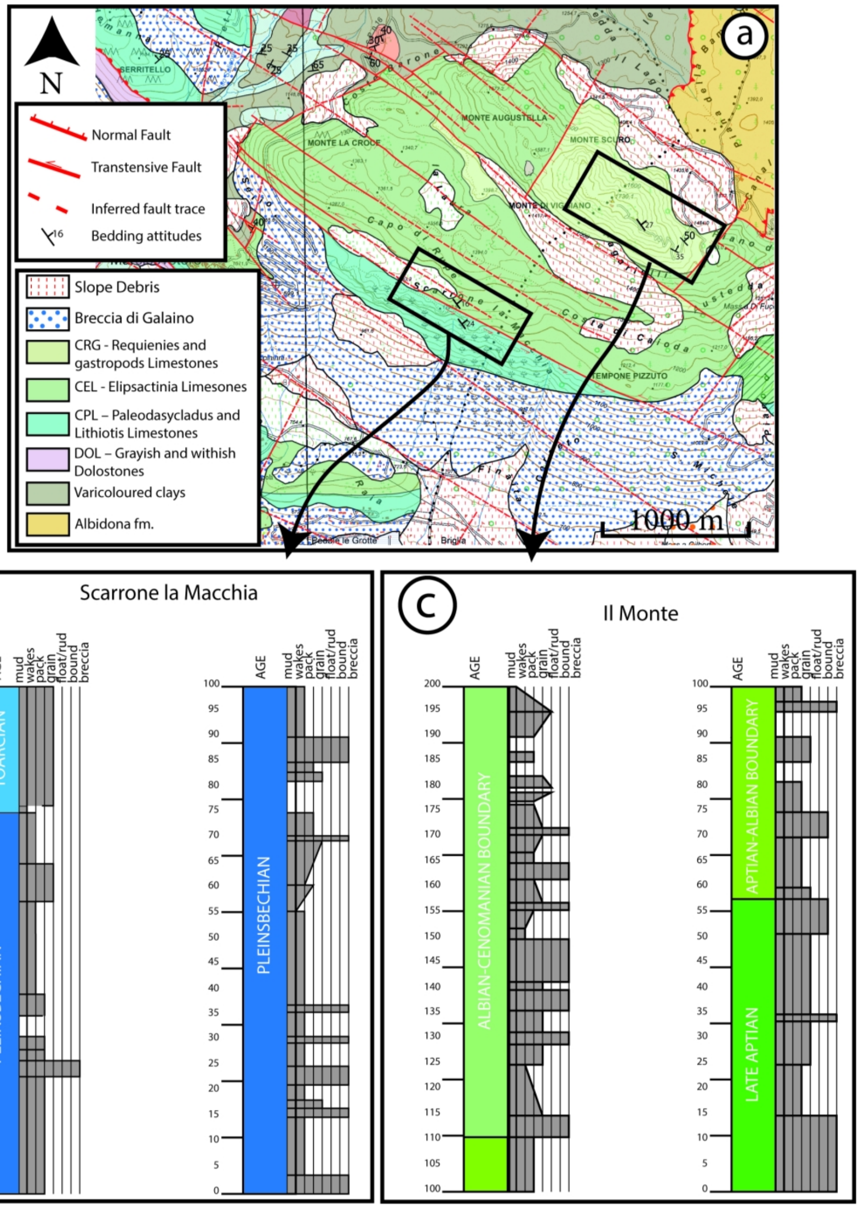
a
N
Normal Fault
Transtensive Fault
Inferred fault trace
Bedding attitudes
Slope Debris
Breccia di Galaino
CRG - Requienies and gastropods Limestones
CEL - Elipsactinia Limesones
CPL – Paleodasycladus and Lithiotis Limestones
DOL – Grayish and withish Dolostones
Varicoloured clays
Albidona fm.
MONTE AUGUSTELLA
MONTE LA CROCE
MONTE SCURO
TEMPONE PIZZUTO
1000 m
b
Scarrone la Macchia
AGE
mud
wakes
pack
grain
float/rud
bound
breccia
TOARCIAN
PLEINSBECHIAN
c
Il Monte
ALBIAN-CENOMANIAN BOUNDARY
APTIAN-ALBIAN BOUNDARY
LATE APTIAN

Figure 2

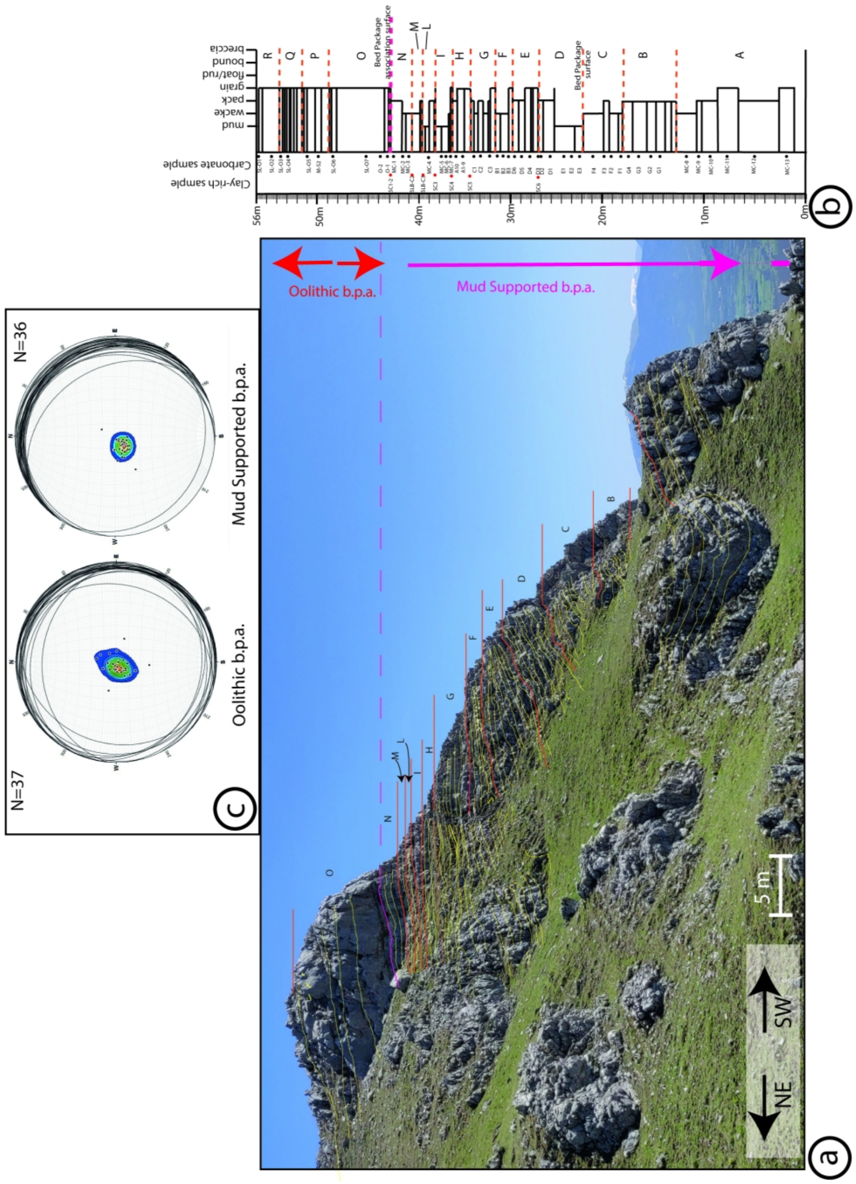
Oolithic b.p.a.
Mud Supported b.p.a.
N=36
N=37
5 m
NE
SW
Carbonate sample
Clay-rich sample
mud
wacke
pack
grain
float/rud
bound
breccia
Bed Package association surface
Bed Package surface
56m
50m
40m
30m
20m
10m
0m

Figure 3a-c


e
carbonate sample
mud
wacke
pack
grain
float/rud
bound
breccia
Bed Package association surface
Bed Package surface
67m
60m
50m
40m
30m
20m
10m
0m
d
5 m
S
N
f
Breccia b.p.a.
N=56

Figure 3d-f

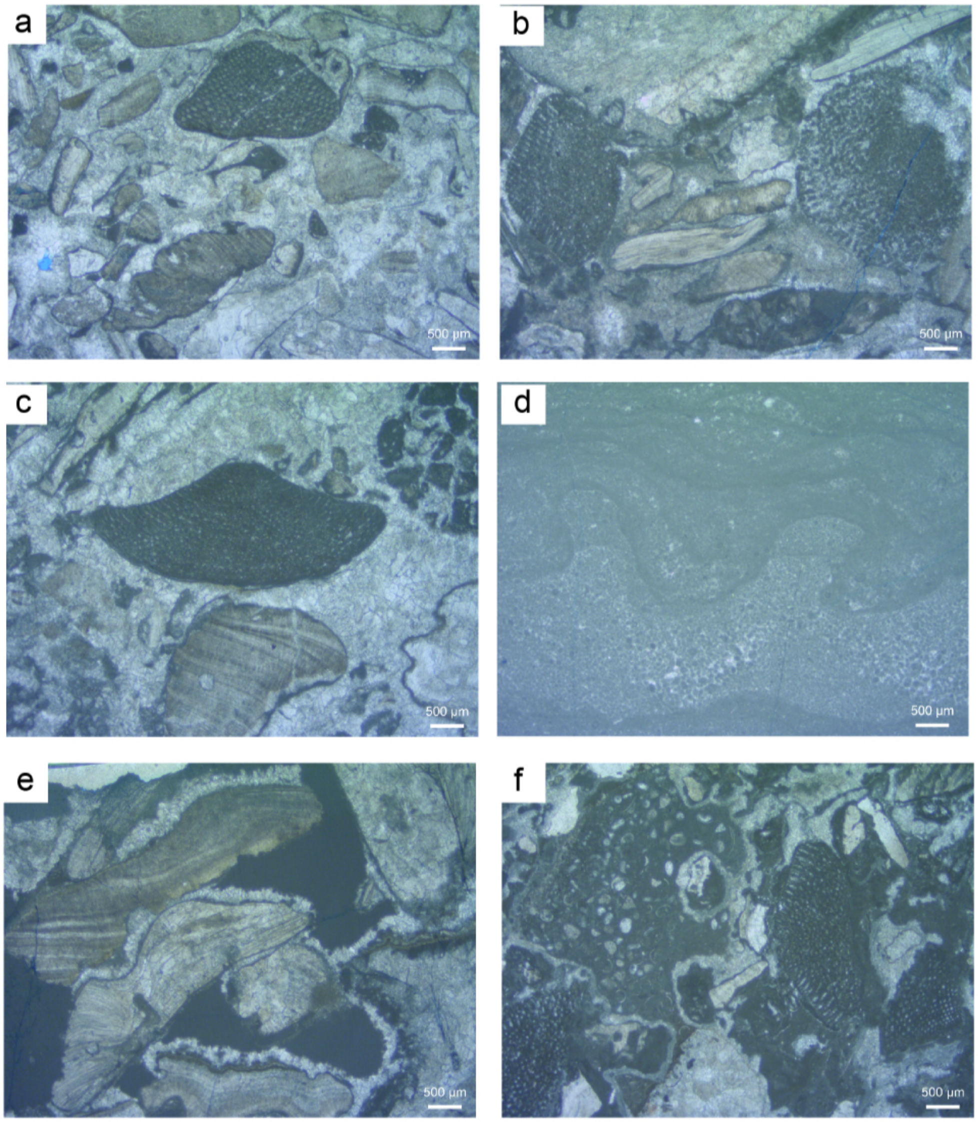

Figure 5

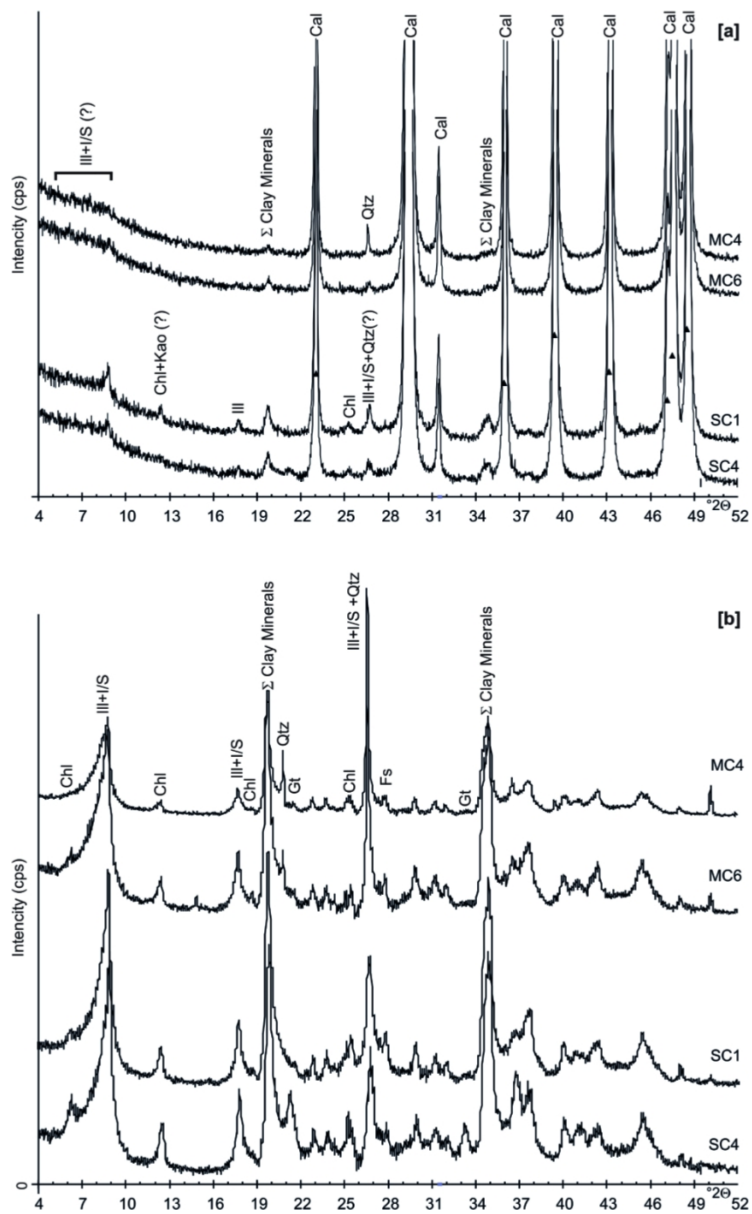

[a]
[b]
Intencity (cps)
Cal
Qtz
Σ Clay Minerals
Ill+I/S (?)
Chl+Kao (?)
Ill
Chl
Ill+I/S+Qtz(?)
Ill+I/S
Ill+I/S +Qtz
Gt
Fs
MC4
MC6
SC1
SC4
°2Θ
4 7 10 13 16 19 22 25 28 31 34 37 40 43 46 49 52

Figure 6

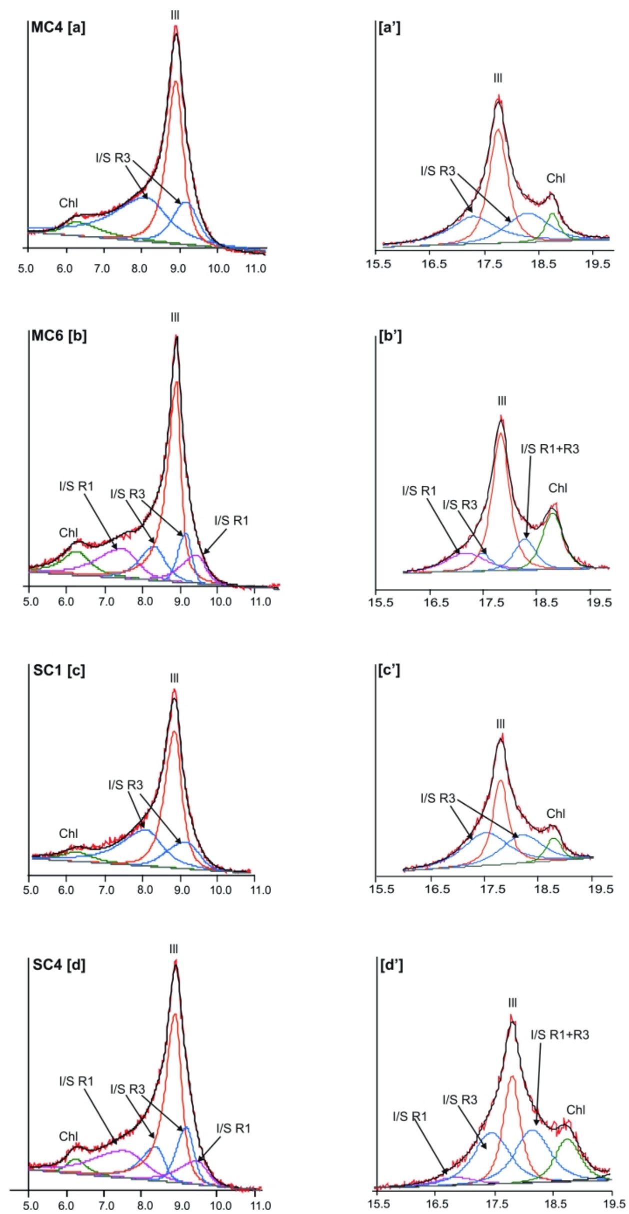
MC4 [a]
Ill
I/S R3
Chl
5.0 6.0 7.0 8.0 9.0 10.0 11.0
[a']
Ill
I/S R3
Chl
15.5 16.5 17.5 18.5 19.5
MC6 [b]
Ill
I/S R1
I/S R3
I/S R1
Chl
5.0 6.0 7.0 8.0 9.0 10.0 11.0
[b']
Ill
I/S R1+R3
I/S R1
I/S R3
Chl
15.5 16.5 17.5 18.5 19.5
SC1 [c]
Ill
I/S R3
Chl
5.0 6.0 7.0 8.0 9.0 10.0 11.0
[c']
Ill
I/S R3
Chl
15.5 16.5 17.5 18.5 19.5
SC4 [d]
Ill
I/S R1
I/S R3
I/S R1
Chl
5.0 6.0 7.0 8.0 9.0 10.0 11.0
[d']
Ill
I/S R1+R3
I/S R3
I/S R1
Chl
15.5 16.5 17.5 18.5 19.5

Figure 7

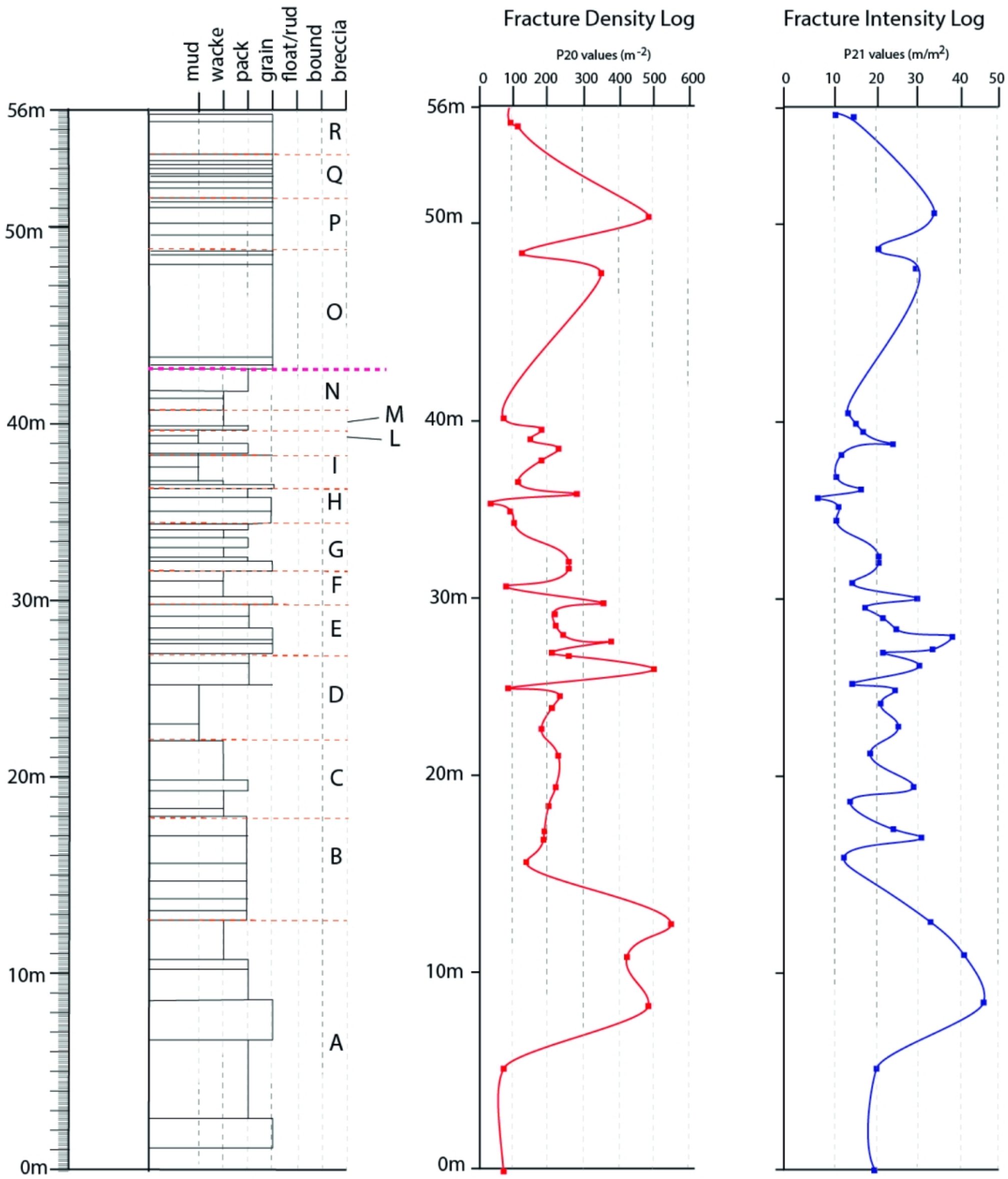
mud
wacke
pack
grain
float/rud
bound
breccia
56m
50m
40m
30m
20m
10m
0m
R
Q
P
O
N
M
L
I
H
G
F
E
D
C
B
A
Fracture Density Log
P20 values (m⁻²)
0 100 200 300 400 500 600
56m
50m
40m
30m
20m
10m
0m
Fracture Intensity Log
P21 values (m/m²)
0 10 20 30 40 50

Figure 8a

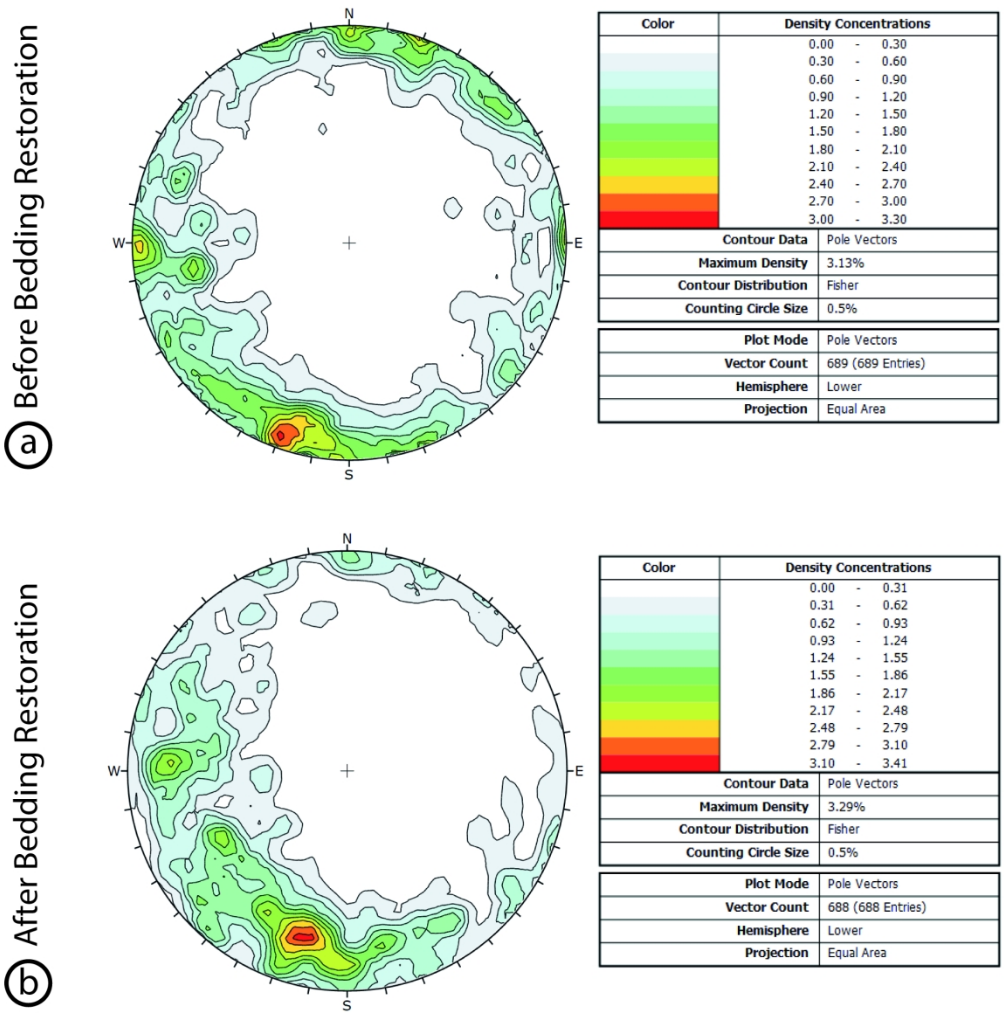
a
Before Bedding Restoration
N
W
E
S
Color
Density Concentrations
0.00 - 0.30
0.30 - 0.60
0.60 - 0.90
0.90 - 1.20
1.20 - 1.50
1.50 - 1.80
1.80 - 2.10
2.10 - 2.40
2.40 - 2.70
2.70 - 3.00
3.00 - 3.30
Contour Data Pole Vectors
Maximum Density 3.13%
Contour Distribution Fisher
Counting Circle Size 0.5%
Plot Mode Pole Vectors
Vector Count 689 (689 Entries)
Hemisphere Lower
Projection Equal Area
b
After Bedding Restoration
N
W
E
S
Color
Density Concentrations
0.00 - 0.31
0.31 - 0.62
0.62 - 0.93
0.93 - 1.24
1.24 - 1.55
1.55 - 1.86
1.86 - 2.17
2.17 - 2.48
2.48 - 2.79
2.79 - 3.10
3.10 - 3.41
Contour Data Pole Vectors
Maximum Density 3.29%
Contour Distribution Fisher
Counting Circle Size 0.5%
Plot Mode Pole Vectors
Vector Count 688 (688 Entries)
Hemisphere Lower
Projection Equal Area

Figure 9

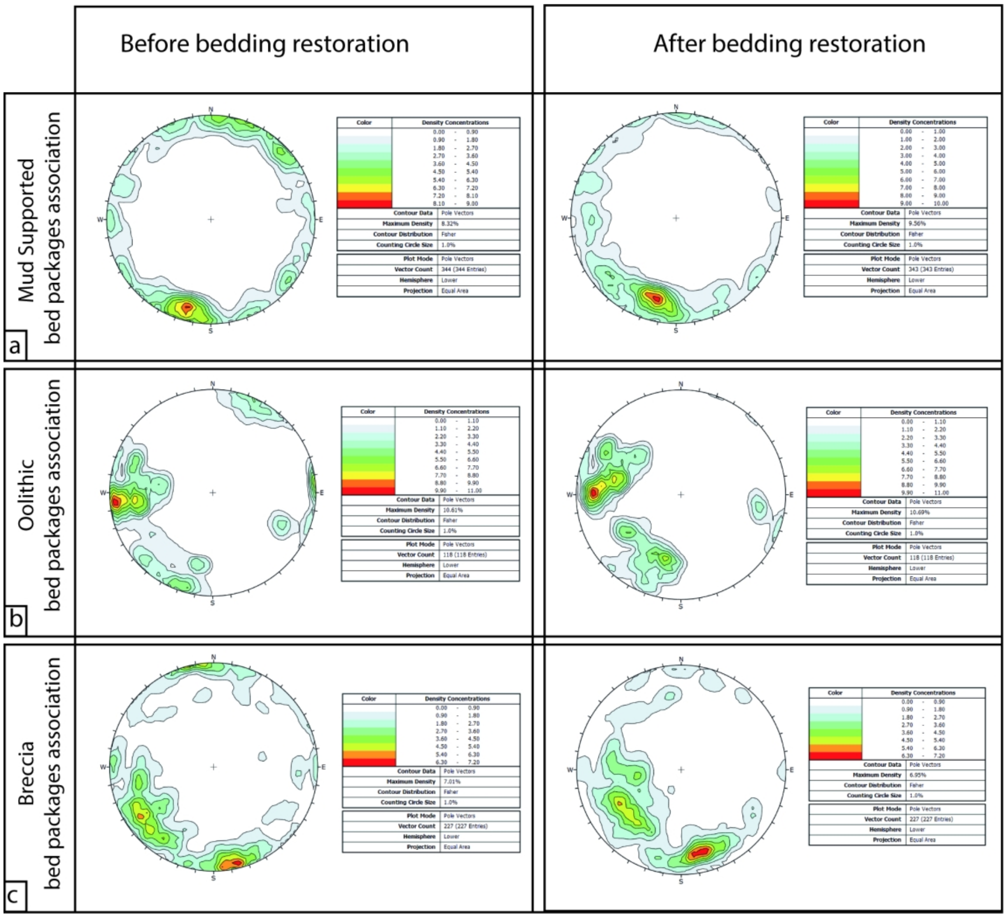
Before bedding restoration
After bedding restoration
Mud Supported bed packages association
Oolithic bed packages association
Breccia bed packages association
a
b
c

Figure 10

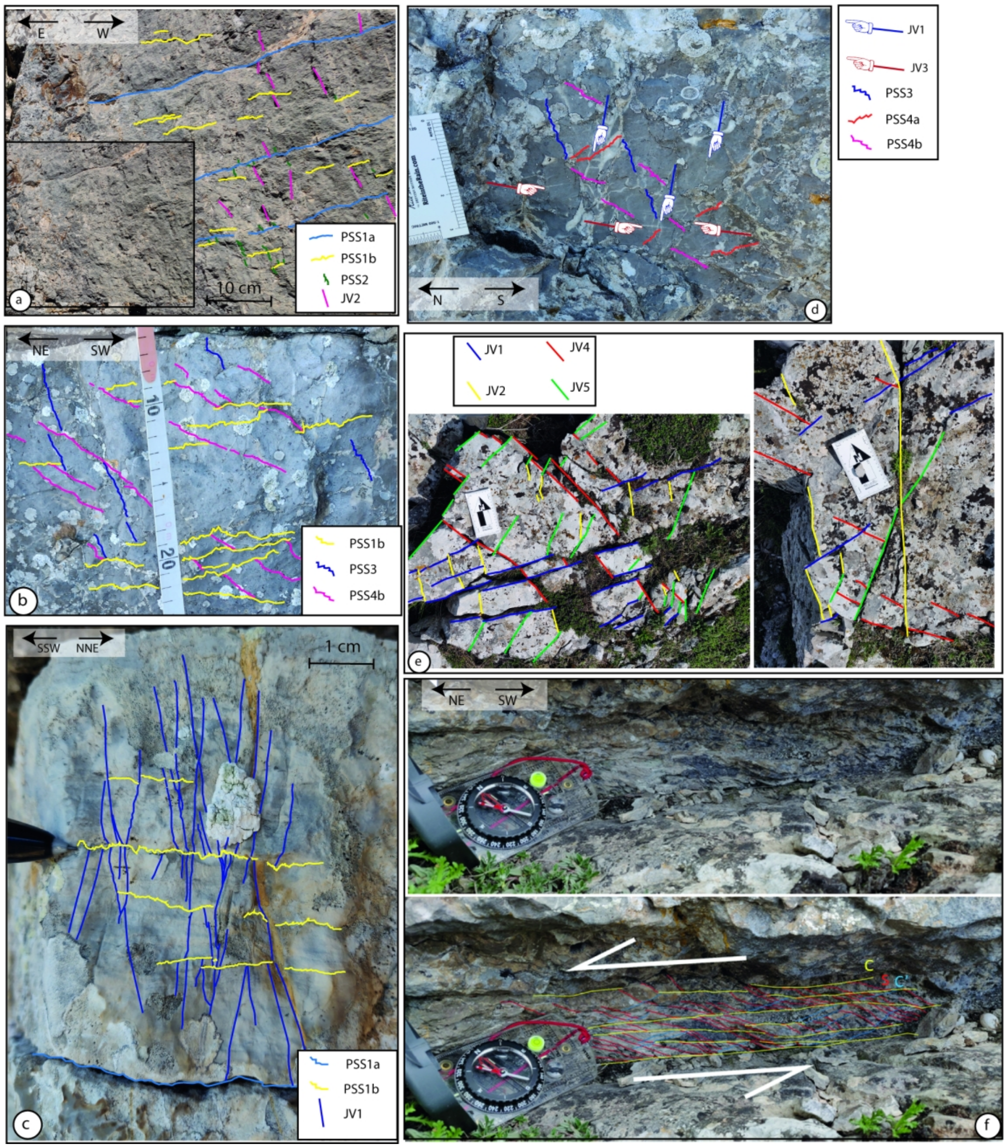
E
W
PSS1a
PSS1b
PSS2
JV2
10 cm
a
N
S
JV1
JV3
PSS3
PSS4a
PSS4b
d
NE
SW
10
20
PSS1b
PSS3
PSS4b
b
JV1
JV4
JV2
JV5
e
SSW
NNE
1 cm
PSS1a
PSS1b
JV1
c
NE
SW
C
f

Figure 11

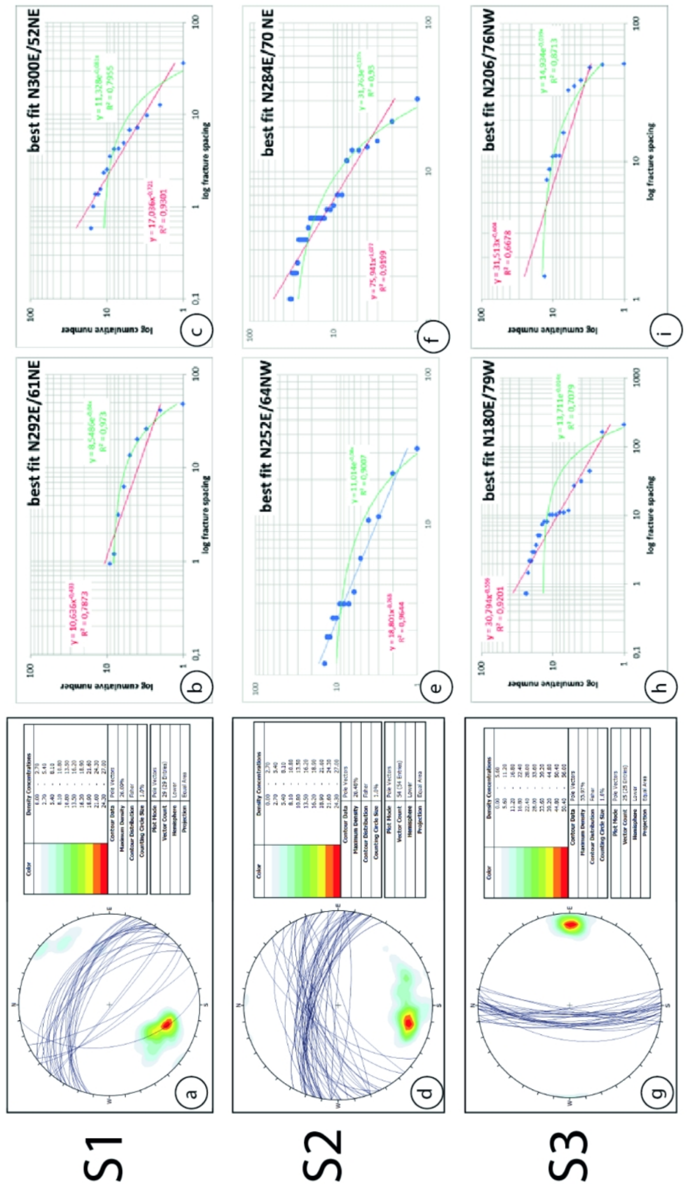
S1
S2
S3
best fit N292E/61NE
best fit N300E/52NE
best fit N252E/64NW
best fit N284E/70 NE
best fit N180E/79W
best fit N206/76NW
log cumulative number
log fracture spacing
a
b
c
d
e
f
g
h
i

Figure 12

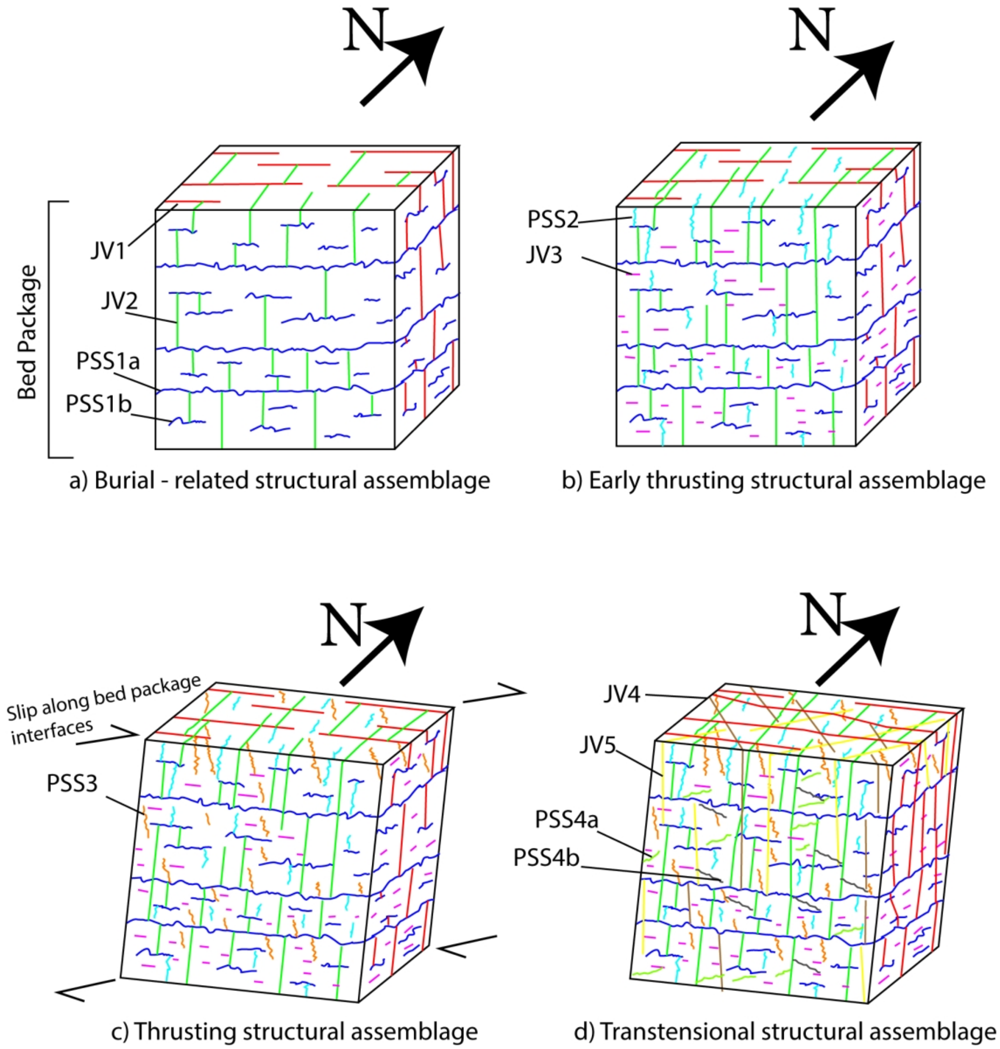
N
Bed Package
JV1
JV2
PSS1a
PSS1b
a) Burial - related structural assemblage
PSS2
JV3
b) Early thrusting structural assemblage
Slip along bed package interfaces
PSS3
c) Thrusting structural assemblage
JV4
JV5
PSS4a
PSS4b
d) Transtensional structural assemblage

Figure 13